Conformational dependence of the intrinsic acidity of the aspartic acid residue sidechain in N-acetyl-*L*-aspartic acid-N'-methylamide

Joseph C. P. Koo

A dissertation submitted in conformity with the requirements of the Ph.D. degree

Department of Pharmacology and Pharmacotherapy
University of Szeged
Szeged, Hungary

2002

Conformational dependence of the intrinsic acidity of the aspartic acid residue sidechain in N-acetyl-*L*-aspartic acid-N'-methylamide

Joseph C. P. Koo

A dissertation submitted in conformity with the requirements of the Ph.D. degree

Department of Pharmacology and Pharmacotherapy
University of Szeged
Szeged, Hungary

2002

ABSTRACT

Conformational analyses have been carried out on the *endo* and *exo* forms of the carboxylic acid-containing sidechain of the aspartic acid residue as well as their deprotonated forms, the aspartate ion. The 3 x 3 = 9 backbone and 3 x 3 = 9 sidechain conformations lead to a grand total of 9 x 9 = 81 structures.

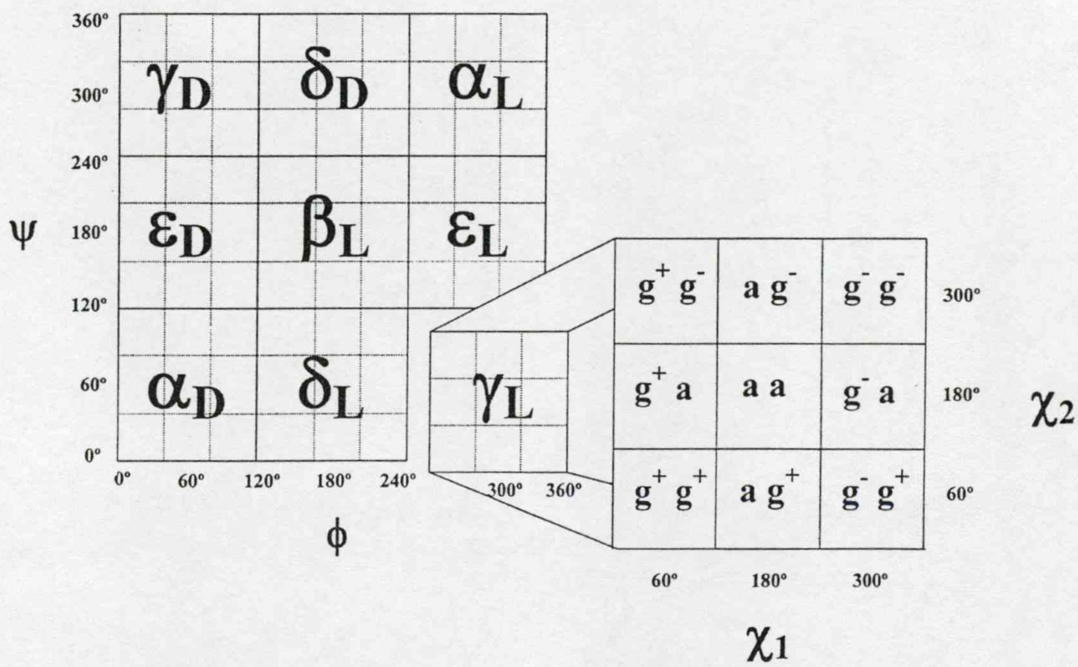

Considerably fewer than 81 structures were found; 37 *endo* and 27 *exo* for the aspartic acid residue as well as 7 for the aspartate ion. Unexpected α_L and ε_L conformations were found in the cases of the aspartic acid residue. For the aspartate residue the three conformers were located in the α_L conformation, one of which was the global minimum.

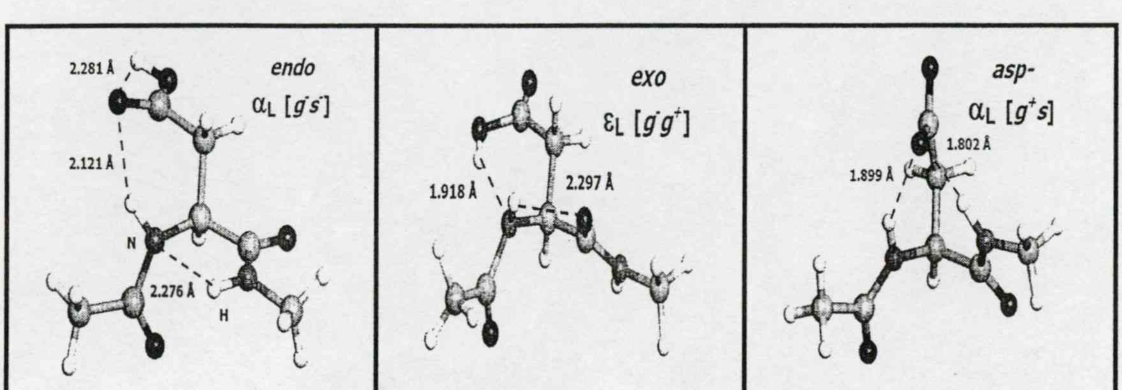

It seemed that the aspartic acid residue would rather change conformation to the favourable backbone structures (γ_L, β_L, α_L, α_D) before it would undergo deprotonation. A conformer of the aspartic acid residue, in any of the δ_L, ε_L, γ_D, δ_D, and ε_D backbone conformations, would migrate to one of its nearest neighbours by changing either the ϕ or the ψ torsional angle prior to deprotonation.

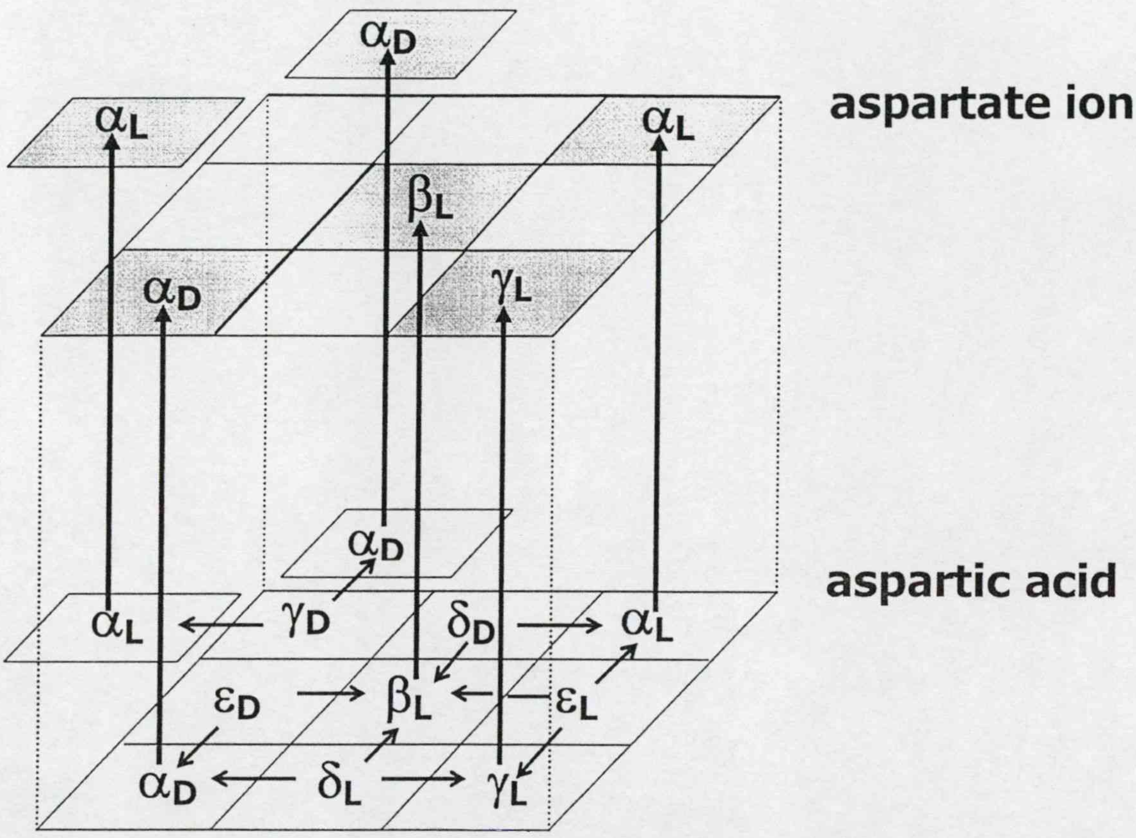

Deprotonation Scheme of Aspartic Acid Residue to Aspartate Ion

DISCLAIMER

The present dissertation is concerned with the conformational intricacies of the aspartic acid residue, one of two amino acids that has a carboxylic acid sidechain.

Not all aspects of the conformational change or the energetics of deprotonation is studied. The present dissertation, however, represents a "progress report" which hopefully shows the direction for further studies.

TABLE OF CONTENTS

Title Page	(i)
Abstract	(ii)
Disclaimer	(iv)
Table of Contents	(v)
List of Tables	(vi)
List of Figures	(viii)
Acknowledgements	(xii)
Publisher Papers	(xiii)
1. Introduction	1
1.1 Overview	1
1.2 Biological Background	1
1.3 Conformational Background	4
2. Choice of Topic	10
3. Aim of Study	11
4. Method	12
4.1 Gaussian Computations	12
4.2 Stabilization Energies	13
5. Results and Discussions	15
5.1 Aspartic Acid	15
5.1.1 *Endo* Form of Aspartic Acid	15
5.1.1.1 Molecular Geometry of the *Endo* Form of Aspartic Acid	15
5.1.1.2 Molecular Energetics of the *Endo* Form of Aspartic Acid	22
5.1.2 *Exo* Form of Aspartic Acid	23
5.1.2.1 Molecular Geometry of the *Exo* Form of Aspartic Acid	23
5.1.2.2 Molecular Energetics of the *Exo* Form of Aspartic Acid	31
5.2 Aspartate Ion	31
5.2.1 Molecular Geometry of the Aspartate Ion	31
5.2.2 Molecular Energetics of the Aspartate Ion	36
5.3 Intrinsic Sidechain Acidity of Aspartic Acid Residue	37
6. Conclusions	44
6.1 Aspartic Acid	44
6.1.1 *Endo* Form of Aspartic Acid	44
6.1.2 *Exo* Form of Aspartic Acid	45
6.2 Aspartate Ion	46
7. References	47
8. Appendix (Published and Accepted Papers)	51

LIST OF TABLES

Table 1:
Optimized energies (hartree) of the various components in the isodesmic reactions used in the calculation of stabilization energy values at the B3LYP/6-31G(d) level of theory.

Table 2:
Optimized conformers of N-acetyl-*L*-aspartic acid N'-methylamide in its *endo* form for all its stable backbone (γ_L, β_L, δ_L, α_L, γ_D, δ_D, α_D, and ε_D) conformations computed at the B3LYP/6-31G(d) level of theory. Shown here are the optimized torsional angles, computed energy values, relative energies, and stabilization energies.

Table 3:
The relative distances of intramolecular hydrogen bonds of N-acetyl-*L*-aspartic acid N'-methylamide in its *endo* form for all its stable backbone (γ_L, β_L, δ_L, α_L, γ_D, δ_D, α_D, and ε_D) conformations computed at the B3LYP/6-31G(d) level of theory. No conformers were found for the ε_L backbone and hence no hydrogen bond distances for the ε_L backbone could be tabulated.

Table 4:
Optimized conformers of N-acetyl-*L*-aspartic acid N'-methylamide in its *exo* form for all its stable backbone (γ_L, β_L, δ_L, ε_L, γ_D, δ_D, α_D, and ε_D) conformations computed at the B3LYP/6-31G(d) level of theory. Shown here are the optimized torsional angles, computed energy values, relative energies, and stabilization energies.

Table 5:
The relative distances of potential hydrogen bonds of N-acetyl-*L*-aspartic acid N'-methylamide in its *exo* form for all its stable backbone (γ_L, β_L, δ_L, ε_L, γ_D, δ_D, α_D, and ε_D) conformations computed at the B3LYP/6-31G(d) level of theory. No conformers were found for the α_L backbone and hence no hydrogen bond distances for the α_L backbone could be tabulated.

Table 6:
Geometric and energetic parameters of optimized conformers of N-acetyl-*L*-aspartate-N'-methylamide for all its stable backbone (γ_L, β_L, α_L, and α_D) conformations computed at the B3LYP/6-31G(d) level of theory. Shown here are the optimized torsional angles, computed energy values, relative energies, and stabilization energies.

Table 7:
Deprotonation energies found for the *endo* and *exo* conformers of N-acetyl-*L*-aspartic acid-N'-methylamide against conformers optimized for N-acetyl-*L*-aspartate-N'-methylamide in the γ_L backbone conformation at the B3LYP/6-31G(d) level of theory.

Table 8:
Deprotonation energies found for the *endo* and *exo* conformers of N-acetyl-*L*-aspartic acid-N'-methylamide against conformers optimized for N-acetyl-*L*-aspartate-N'-methylamide in the β_L backbone conformation at the B3LYP/6-31G(d) level of theory.

Table 9:
Deprotonation energies found for the *endo* and *exo* conformers of N-acetyl-*L*-aspartic acid-N'-methylamide against conformers optimized for N-acetyl-*L*-aspartate-N'-methylamide in the α_L backbone conformation at the B3LYP/6-31G(d) level of theory.

Table 10:
Deprotonation energies found for the *endo* and *exo* conformers of N-acetyl-*L*-aspartic acid-N'-methylamide against conformers optimized for N-acetyl-*L*-aspartate-N'-methylamide in the α_D backbone conformation at the B3LYP/6-31G(d) level of theory.

Table 11:
The relative distances of potential hydrogen bonds of N-acetyl-*L*-aspartate-N'-methylamide for all its stable backbone (γ_L, β_L, α_L, and α_D) conformations computed at the B3LYP/6-31G(d) level of theory. No conformers were found for the δ_L, ε_L, γ_D, δ_D, and ε_D backbone conformations and hence no hydrogen bond distances for these backbones could be tabulated.

LIST OF FIGURES

Figure 1:
A preliminary optimization[41] of the Arginine (R)-Glyince (G)-Aspartic Acid (D) [RGD] tripeptide.

Figure 2:
Definition of torsional angles and atomic numbering for (left) the *endo* form and (right) the *exo* form of N-acetyl-*L*-aspartic acid N'-methylamide.

Figure 3:
The 2D topology of a Ramachandran potential energy surface (PEHS), E = E (ϕ, ψ) of an amino acid residue in a peptide. (Left) Conformers are designated by IUPAC conventions; (right) conformers are designated by traditional conventions.

Figure 4:
A schematic representation of the 4D Ramachandran PEHS, E = E (ϕ, ψ, χ_1, χ_2). Each of the nine backbone conformations (γ_L, β_L, δ_L, α_L, ε_L, γ_D, δ_D, α_D, ε_D) has nine sidechain conformations as shown by the γ_L conformation.

Figure 5:
Deprotonation of N-acetyl-*L*-aspartate-N'-methylamide (top) to the *endo* (bottom left) or the *exo* (bottom right) forms of N-acetyl-*L*-aspartic acid-N'-methylamide.

Figure 6:
Definitions of atomic numbering and torsional angles for N-acetyl-*L*-aspartate-N'-methylamide.

Figure 7:
Deprotonation choices for N-acetyl-*L*-aspartic acid-N'-methylamide: [1] and [4] depicts the protonated *exo* form while [2] and [3] depicts the protonated *endo* form. The two *exo* forms (and the two *endo* forms) differ from one another by having their χ_2 torsional angles rotated by 180°.

Figure 8:
Schematic representation of the title compounds.

Figure 9:
Schematic representation of the vertical and adiabatic deprotonation energies (or proton affinities).

Figure 10:
Definition of stabilization energies of the *endo* form of N-acetyl-*L*-aspartic acid N'-methylamide with respect to the γ_L or β_L conformer of N-acetyl glycine N' methylamide.

Figure 11:
Landscape representation of the nine sidechain conformational PEHSs, E = E (χ_1, χ_2) associated with each one of the nine backbone conformations for the *endo* form of the aspartic acid residue. Torsional angles χ_1 and χ_2 are given in degrees from 0° to 360°.

Figure 12:
Contour representation of the nine sidechain conformational PEHSs, E = E (χ_1, χ_2) associated with each one of the nine backbone conformations for the *endo* form of the aspartic acid residue. Torsional angles χ_1 and χ_2 are given in degrees from 0° to 360°.

Figure 13:
Classification of the types of internal hydrogen bonding for the *endo* form of N-acetyl-*L*-aspartic acid N'-methylamide.

Figure 14:
A new type of backbone-backbone (—CON—H⋯⋯ NHCO—) hydrogen bonding observed in the case of the α_L [g^- s^-] conformation at H⋯⋯ Ndistance of 2.276 Å in addition to regular hydrogen bonds for the *endo* form of the aspartic acid residue.

Figure 15:
A trend showing the interrelation between hydrogen-bonded distance and ring size (RS) of internal hydrogen bonds for the *endo* form of N-acetyl-*L*-aspartic acid N'-methylamide.

Figure 16:
Landscape representation of the nine sidechain conformational PEHSs, E = E (χ_1, χ_2) associated with each one of the nine backbone conformations for the *exo* form of N-acetyl-*L*-aspartic acid N'-methylamide. Torsional angles χ_1 and χ_2 are given in degrees from 0° to 360°.

Figure 17:
Contour representation of the nine sidechain conformational PEHSs, E = E (χ_1, χ_2) associated with each one of the nine backbone conformations for the *exo* form of N-acetyl-*L*-aspartic acid N'-methylamide. Torsional angles χ_1 and χ_2 are given in degrees from 0° to 360°.

Figure 18:
A graphical representation of the stable conformer found at g^- g^+ of the ε_L backbone of the *exo* form of the aspartic acid residue.

Figure 19:
Classification of the types of internal hydrogen bonding for the *exo* form of N-acetyl-*L*-aspartic acid N'-methylamide.

Figure 20:
A trend showing the interrelation between hydrogen-bonded distance and ring size (RS) of internal hydrogen bonds for the *exo* form of N-acetyl-*L*-aspartic acid N'-methylamide.

Figure 21:
Double-scan PES, E = E (χ_1, χ_2), generated for the γ_L backbone conformation of: (a) the *endo* form of N-acetyl-*L*-aspartic acid-N'-methylamide, (b) N-acetyl-*L*-aspartate-N'-methylamide, (c) the *exo* form of N-acetyl-*L*-aspartic acid-N'-methylamide in both landscape (top) and contour (bottom) representations. Torsional angles χ_1 and χ_2 are given in degrees from 0° to 360°.

Figure 22:
Double-scan PES, E = E (χ_1, χ_2), generated for the β_L backbone conformation of: (a) the *endo* form of N-acetyl-*L*-aspartic acid-N'-methylamide, (b) N-acetyl-*L*-aspartate-N'-methylamide, (c) the *exo* form of N-acetyl-*L*-aspartic acid-N'-methylamide in both landscape (top) and contour (bottom) representations. Torsional angles χ_1 and χ_2 are given in degrees from 0° to 360°.

Figure 23:
Double-scan PES, E = E (χ_1, χ_2), generated for the α_L backbone conformation of: (a) the *endo* form of N-acetyl-*L*-aspartic acid-N'-methylamide, (b) N-acetyl-*L*-aspartate-N'-methylamide, (c) the *exo* form of N-acetyl-*L*-aspartic acid-N'-methylamide in both landscape (top) and contour (bottom) representations. Torsional angles χ_1 and χ_2 are given in degrees from 0° to 360°.

Figure 24:
Double-scan PES, E = E (χ_1, χ_2), generated for the α_D backbone conformation of: (a) the *endo* form of N-acetyl-*L*-aspartic acid-N'-methylamide, (b) N-acetyl-*L*-aspartate-N'-methylamide, (c) the *exo* form of N-acetyl-*L*-aspartic acid-N'-methylamide in both landscape (top) and contour (bottom) representations. Torsional angles χ_1 and χ_2 are given in degrees from 0° to 360°.

Figure 25:
A graphical representation of the global minimum found at the α_L [g^+ *s*] backbone conformation of the aspartate residue.

Figure 26:
Scatter-plot diagrams showing the optimized conformers found for N-acetyl-*L*-aspartate-N'-methylamide and the *endo* and *exo* forms of N-acetyl-*L*-aspartic acid-N'-methylamide in the γ_L, α_L, α_D, and β_L backbone conformations. Note: rhombus represents N-acetyl-*L*-aspartate-N'-methylamide, circle represents the *endo* form of N-acetyl-*L*-aspartic acid-N'-methylamide, and triangles represent the *exo* form of N-acetyl-*L*-aspartic acid-N'-methylamide

Figure 27:
Classification of the "traditional" hydrogen bond interactions for N-acetyl-*L*-aspartate-N'-methylamide.

Figure 28:
Double-scan PES, E = E (χ_1, χ_2), generated for the deprotonation energies of (a) the *endo*, (b) the average deprotonation energies of both the *endo* and the *exo* forms, and (c) the *exo* forms of N-acetyl-*L*-aspartic acid-N'-methylamide in its γ_L backbone conformation. Torsional angles χ_1 and χ_2 are given in degrees from 0° to 360°.

Figure 29:
Double-scan PES, E = E (χ_1, χ_2), generated for the deprotonation energies of (a) the *endo*, (b) the average deprotonation energies of both the *endo* and the *exo* forms, and (c) the *exo* forms of N-acetyl-*L*-aspartic acid-N'-methylamide in its β_L backbone conformation. Torsional angles χ_1 and χ_2 are given in degrees from 0° to 360°.

Figure 30:
Double-scan PES, E = E (χ_1, χ_2), generated for the deprotonation energies of (a) the *endo*, (b) the average deprotonation energies of both the *endo* and the *exo* forms, and (c) the *exo* forms of N-acetyl-*L*-aspartic acid-N'-methylamide in its α_L backbone conformation. Torsional angles χ_1 and χ_2 are given in degrees from 0° to 360°.

Figure 31:
Double-scan PES, E = E (χ_1, χ_2), generated for the deprotonation energies of (a) the *endo*, (b) the average deprotonation energies of both the *endo* and the *exo* forms, and (c) the *exo* forms of N-acetyl-*L*-aspartic acid-N'-methylamide in its α_D backbone conformation. Torsional angles χ_1 and χ_2 are given in degrees from 0° to 360°.

Figure 32:
A schematic representation of the backbone conformational change of aspartic acid residue prior to sidechain deprotonation to the corresponding aspartate residue. Shaded areas represent stable aspartate conformations.

Figure 33:
A schematic representation of the various hydrogen bond interactions that may exist in the *endo* form of the aspartic acid residue.

Figure 34:
A schematic diagram showing the various hydrogen bond interaction that may exist for the *exo* form of the aspartic acid residue.

Figure 35:
Deprotonation scheme of aspartic acid residue to aspartate ion.

ACKNOWLEDGEMENTS

The author wishes to acknowledge the encouragement and moral support of Dr. Julius Gy. Papp. The author is also grateful to Ms. Janice. S. W. Lam, Dr. Gregory A. Chass, Dr. Ladislaus L. Torday, and Professor I.G. Csizmadia for their inspiration and guidance during this research as well as during the preparation of this dissertation.

PUBLISHED PAPERS

1. **Joseph C. P. Koo**, Gregory A. Chass, Andras Perczel, Ödon Farkas, Ladislaus L. Torday, Andras Varro, Julius Gy. Papp, and Imre G. Csizmadia. Exploration of the 4D-conformational potential energy hypersurface of N-acetyl-L-aspartic acid-N'-methylamide with its internally hydrogen bonded sidechain orientation, J. Phys. Chem. A, 106 (**2002**), 6999-7009.

   IF: **2.630**

2. **Joseph C. P. Koo**, Gregory A. Chass, Andras Perczel, Ödon Farkas, Ladislaus L. Torday, Andras Varro, Julius Gy. Papp, and Imre G. Csizmadia. N-acetyl-L-aspartic acid-N'-methylamide with sidechain orientation capable of external hydrogen bonding. Backbone and sidechain folding, studied at the DFT level of quantum theory, Eur. Phys. J. D, 20 (**2002**), 499-511.

   IF: **1.583**

3. **Joseph C. P. Koo**, Janice S.W. Lam, Gregory A. Chass, Salvatore J. Salpietro, R. Daniel Enriz, Ladislaus L. Torday, Andras Varro, and Julius Gy. Papp. How Reliable Could Economic Hartree-Fock Computations Be In Studying Large, Folded Peptides? A comparative HF and DFT study on N- and C-protected aspartic acid, THEOCHEM **2002** (in press)

   IF: **0.919**

4. **Joseph C. P. Koo**, Janice S.W. Lam, Gregory A. Chass, Ladislaus L. Torday, Andras Varro, and Julius Gy. Papp. Conformational dependence of the intrinsic acidity of the aspartic acid residue sidechain in N-acetyl-*L*-aspartic acid-N'-methylamide, THEOCHEM **2002** (in press)

   IF: **0.919**

PUBLISHED AND ACCEPTED PAPERS :

Cumulative IF : 6.051

First Author in : 4

1. Introduction

1.1 Overview

Computational molecular modeling has become a field of great interest in recent years. In particular, computational studies play a dominant role in drug designs as well as functional studies in pharmacology[1-8]. However, results from computational modeling are often limited by computer powers. In addition, the speed at which these results were generated is also determined by the different theories that form the fundamental formulas and equations in these modeling computer programs. For example, in order to generate more accurate results, it is often time consuming to perform computations at the higher levels of theories. In Molecular Quantum Chemistry, the efficiency and accuracy of *ab initio* calculations are restricted by the above-mentioned conditions. It is important to perform *ab initio* studies on peptides, as they are the constituents from which proteins and most of their ligands are formed. All amino acids can now be studied by *ab initio* methods. Many single amino acids have already been subjected to detailed *ab initio* calculations. These attempts include, among others, alanine[9-14], asparagines[15], cysteine[16-17], glycine[18-19], phenylalanine[20-22], proline[23], selenocysteine[24], serine[25-27], and valine[28]. Recently, attempts were made to compile *ab initio* results of all the naturally occurring amino acids together in a database[29]. This type of molecular analysis is necessary to the growing field of computational studies on biological structures, and is essential in advances to proteomic studies. In this dissertation, the molecular structures and geometric preference for the aspartic acid residue and its sidechain deprotonated form are presented.

1.2 Biological Background

It is not difficult to find biological implications involving aspartic acid. On the molecular level, mutational studies, involving the aspartic acid residue, became very popular in the recent years. For example, it was shown that mutations in two aspartate regions of the human immunodeficiency virus-1 (HIV-1) *chemokine coreceptor CXCR4* would reduce the coreceptor's function in enhancing HIV-1 entry into host cells[30]. The aspartic residue is also shown to be clinically important in many situations. In Neurology, the quantity of N-acetylaspartate is a measurement of cellular dysfunction and neuronal loss for stroke patients suffering from cerebral injury[31]. In experiments that explore the issue of aging, it was shown that intake of K and Mg salts of aspartic acid allows rats to survive longer by as much as 30%[32-33].

An ongoing list of biological applications and experiments can be contributed to researches involving aspartic acid, including lipase activities[34], probing for the binding sites of HIV-1 protease[35], immunological antiproliferative experiments[36], protein modification studies in Alzheimer's Disease[37], enzyme kinetics involving bacteria[38], using aspartic acid-specific sites to probe for target proteins in their normal and disease states[39], and protein decomposition that influences the rate of racemization[40]. Results from these studies often indicate that specific conformations of the aspartic acid could lead to variations in the regulation of a biological system.

One notable application of the aspartic acid residue in a biological system is shown in the RGD tripeptide. The RGD tripeptide can be separated into three components, namely, arginine (R), glycine (G), and aspartic acid (D), shown in **Figure 1**[41].

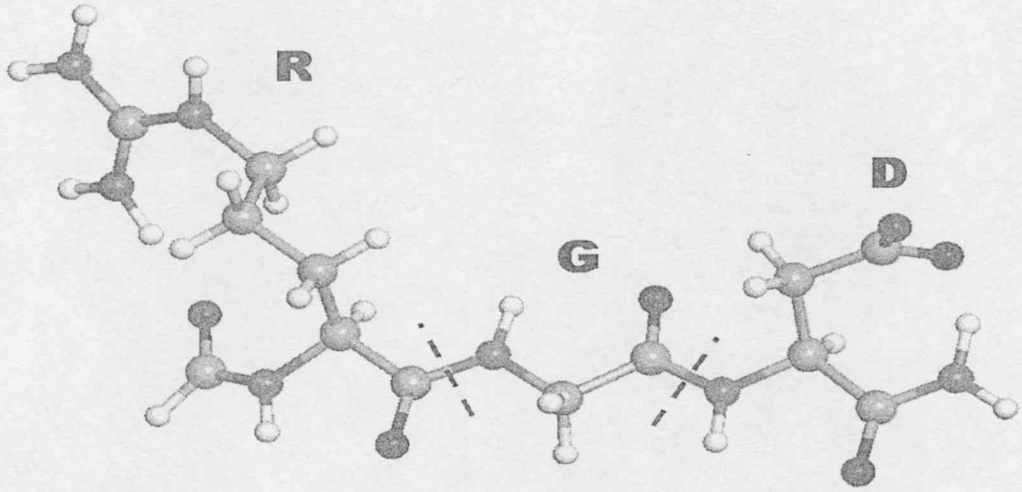

Figure 1 A preliminary optimization[41] of the Arginine (R)-Glycine (G)-Aspartic Acid (D) [RGD] tripeptide.

RGD is highly involved in molecular genetics and cell biology studies, including cell-surface recognition by receptors[42], expanding adenovirus vector tropism[43] and improving gene delivery [44-45] in gene therapy, apoptosis[46], and increasing oral bioavailability in drug production[47]. By exploring the conformation preferences of the aspartic acid (D) residue, one can examine the stabilization forces as well as the molecular geometry for the RGD tripeptide.

Recently, many mutational studies were performed on receptors and channels in the biological systems. Among these investigations were reports that aspartic acid, or aspartate, is crucial in the selectivity and regulation of ion channel selectivity, ligand binding, as well as the functionality of a receptor protein. For instance, it was reported that an aspartic acid site in the inositol 1,4,5-trisphosphate receptor is important in controlling Ca^{2+} selectivity[48]. Also, an aspartate-rich region in the calsequestrin Ca^{2+} binding protein was found to be important in a receptor-mediated Ca^{2+} release process by acting as a direct binding site for Ca^{2+} [49]. In another study, point mutations of the aspartate residue was also found to abolish Ca^{2+} permeation in the epithelial Ca^{2+} channel, causing the channel to be non-functional[50].

Since computational molecular modeling is an area of high interest in recent years in drug designs[1-8], *ab initio* studies on amino acids such as the aspartate residue may deem beneficial in the pharmaceutical industry; especially when exploring binding affinity or selectivity of a target receptor. In this dissertation, all possible sidechain (SC) and backbone (BB) conformers that may exist for the aspartate residue, using N-acetyl-*L*-aspartic acid-N'-methylamide as a peptide model, will be reported. In addition, the deprotonation of the aspartic acid and protonation preference for the aspartate residue will be explored. The deprotonation and protonation characteristics of these residues will predetermine the various inter- and intra-residual interactions that may result from hydrogen bonding. In turn, these forces may directly govern the binding patterns of ligands to aspartate sites in receptors and proteins.

1.3 Conformational Background

An earlier study performed by Salpietro *et al.*[51] focused on the sidechain potential energy surface of **N**-formyl-*L*-aspartic acidamide and its conjugate base **N**-formyl-*L*-aspartamide in their γ_L backbone conformations. In that study, *ab initio* calculations were performed on all sidechain conformations at the γ_L backbone fold of the parent aspartic acid diamide and its conjugate base, the depronated sidechain. Propionic acid and propionate ion were respectively used to mimic the sidechain of **N**-formyl-*L*-aspartamide in its neutral and anionic form. In this dissertation, the full backbone (BB) and sidechain (SC) conformations of **N**-acetyl-*L*-aspartic acid **N'**-methylamide in both *endo* and *exo* forms were explored for the carboxylic acid moiety.

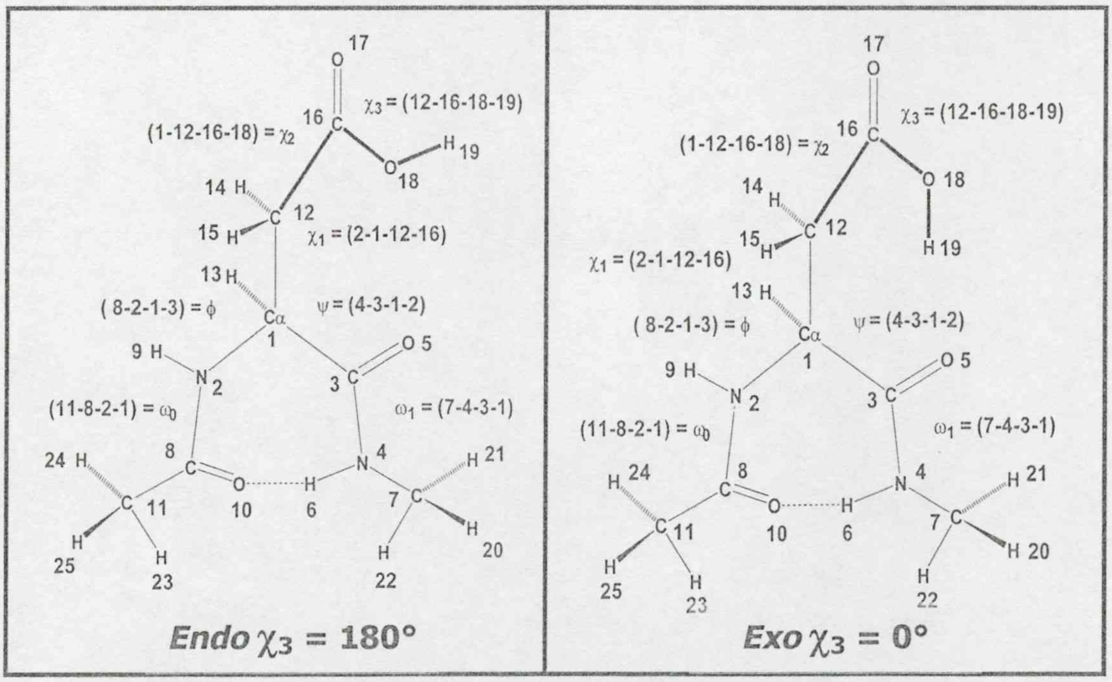

Figure 2 Definition of torsional angles and atomic numbering for (left) the *endo* form and (right) the *exo* form of N-acetyl-*L*-aspartic acid N'-methylamide.

N-acetyl-*L*-aspartic acid N'-methylamide differs from N-formyl-*L*-aspartic acidamide by having methyl groups instead of H atoms in each of its **N**- and **C**-protective groups, as shown in **Figure 2**. It is expected that the backbone geometry of N-acetyl-*L*-aspartic acid **N'**-methylamide will be analogous to that of an alanine residue in a peptide. In this case, however, an H atom of the α- methyl group in alanine is replaced with a –COOH group. Similarly, the backbone geometry of **N**-acetyl-*L*-aspartate-**N'**-methylamide is similar to that of the alanine residue, where the H atom of the α-methyl group of alanine is replaced by a $-COO^-$ group.

Previous studies on the alanine molecule[9-14] did not reveal any stable conformer in either the α_L and ε_L backbones. Because alanine is the simplest chiral amino acid whose backbone also recurred in other peptide residues, it was predicted, at first, that no stable α_L and ε_L conformers will exist N-acetyl-*L*-aspartic acid N'-methylamide.

All naturally occurring amino acids, with the exception of proline, exhibit the same backbone conformational pattern which is illustrated in **Figure 3**. The conformational classification by g^+, a, g^- corresponds to the IUPAC convention and the subscripted Greek letters are used as symbolic names for the nine backbone conformers.

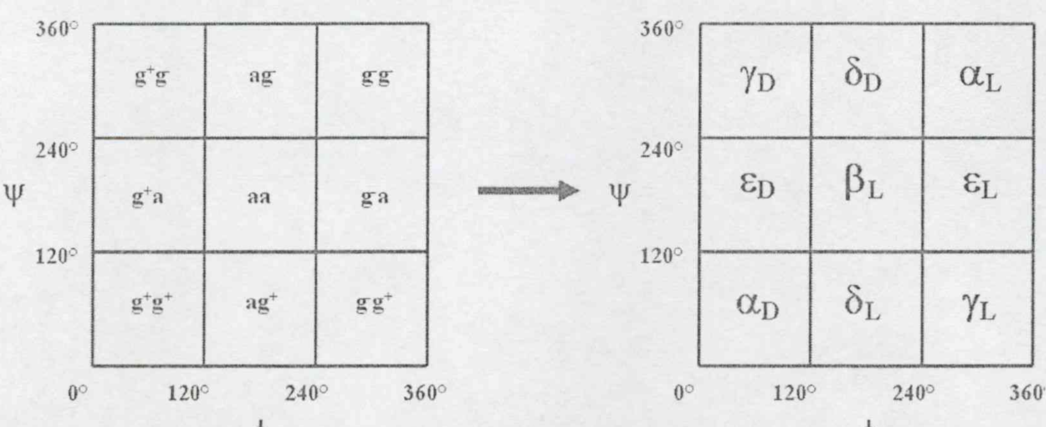

Figure 3 The 2D topology of a Ramachandran potential energy surface (PEHS), E = E (ϕ, ψ) of an amino acid residue in a peptide. (Left) Conformers are designated by IUPAC conventions; (right) conformers are designated by traditional conventions.

In addition to the backbone conformation, the amino acid sidechain may also produce additional conformers. A few of the amino acids have only one torsional angle; for example, valine is a notable case. A relatively large percentage of the amino acids have two sidechain torsional angles (Leu, Ile, Phe, Tyr, Trp, Cys, His, Ser, Thr, Asp, and Asn). The remaining few amino acids have more than two torsional angles (Met, Lys, Arg, Glu, Gln). The focus of the present dissertation is on aspartate ion and aspartic acid residues and therefore the two sidechain torsional angles predetermine the sidechain orientation. Consequently, the 3 x 3 = 9 backbone and the 3 x 3 = 9 sidechain orientations will result in the 9 x 9 = 81 conformations as illustrated by **Figure 4**.

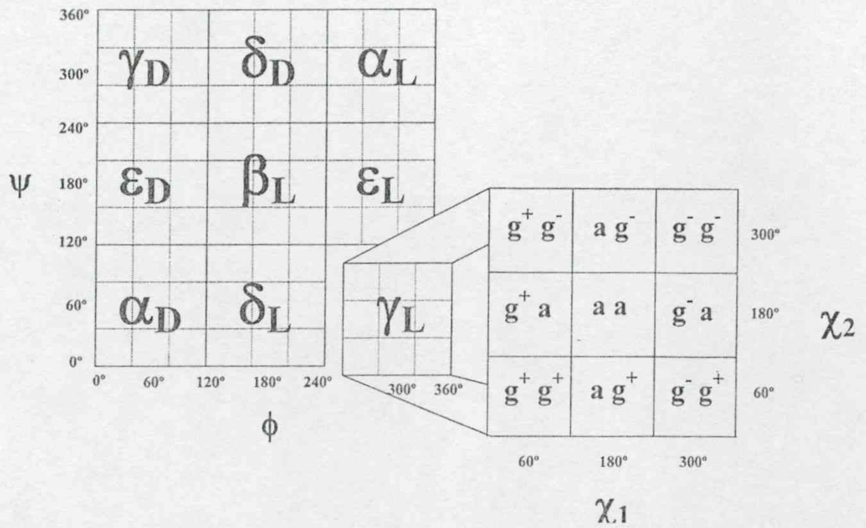

Figure 4 A schematic representation of the 4D Ramachandran PEHS, E = E (ϕ, ψ, χ_1, χ_2). Each of the nine backbone conformations (γ_L, β_L, δ_L, α_L, ε_L, γ_D, δ_D, α_D, ε_D) has nine sidechain conformations as shown by the γ_L conformation.

N-acetyl-*L*-aspartate-N'-methylamide is the deprotonated form of either the *endo* or the *exo* form of N-acetyl-*L*-aspartic acid-N'-methylamide (**Figure 5**).

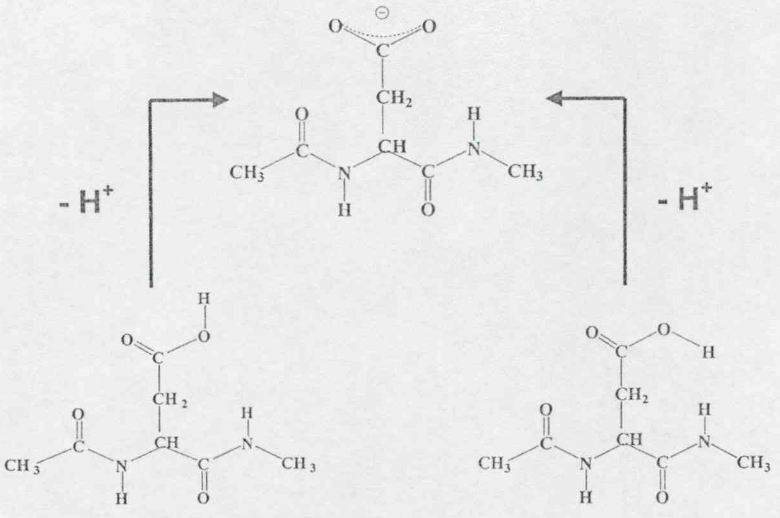

Figure 5 Deprotonation of N-acetyl-*L*-aspartate-N'-methylamide (top) to the *endo* (bottom left) or the *exo* (bottom right) forms of N-acetyl-*L*-aspartic acid-N'-methylamide.

In general, all conformations of an amino acid residue of this complexity may be characterized by at least four torsional angles: ϕ, ψ, χ_1, and χ_2, leading to a potential energy hypersurface (PEHS) consisting of four independent variables (4D) [1]:

$$E = E(\phi, \psi, \chi_1, \chi_2) \qquad [1]$$

In turn, the 4D PEHS can be separated into two distinctive 2D potential energy surfaces (PESs):

$$E = E(\phi, \psi) \qquad [2]$$

$$E = E(\chi_1, \chi_2) \qquad [3]$$

Here, equation [2] denotes the 2D PES for backbone torsional angles (Ramachandran surface) while equation [3] denotes the 2D PES associated with sidechain dihedral angles. Hence, for **N**-acetyl-*L*-aspartate-**N'**-methylamide, both backbone and sidechain torsional angles need to be discussed in relation to the overall PEHS so as to describe the molecular geometry of the aspartate residue. The situation is analogous for the aspartic acid residues but the orientation of the carboxylic sidechain, of *endo* and *exo* forms, may be characterized by an addition torsional angle χ_3.

In this dissertation, optimization results for all stable conformers found in both the *endo* and the *exo* forms of **N**-acetyl-*L*-aspartic acid **N'**-methylamide are reported. Studying the aspartic acid residue in both its *endo* and *exo* forms is important in a biological system (**Figure 2**). For example, in its *exo* form, the peptide residue is allowed to form external hydrogen bonds and when in its *endo* form, these external hydrogen interactions may be broken to allow the formation of other stabilizing forces. These forces are especially important in a biological system involving ligand binding, substrate interactions, protein docking and protein-protein interactions; all of which are pharmacologically important on a molecular level.

The sidechain of the aspartic acid residue can be modeled by propionic acid (CH_3-CH_2-COOH). When χ_3 = 180°, the aspartic acid residue is capable of sidechain-sidechain (SC/SC) internal hydrogen bonding and it is considered to be in an *endo* orientation (**Figure 2**). When $\chi_3 = 0°$, the SC/SC interaction no longer exists and the aspartic acid sidechain is free to participate in external interactions, such as sidechain-backbone (SC/BB) hydrogen bonding. In this case, the aspartic acid residue is considered to be in *exo* orientation (**Figure 2**).

Unlike aspartic acid, there are no *endo* or *exo* orientations in describing the sidechain characteristic of N-acetyl-*L*-aspartate-N'-methylamide. The aspartate anion sidechain can be modeled by propionate (CH_3-CH_2-COO^-) where the α-carbon on the aspartate is represented by CH_3. Here, the carboxylate sidechain of aspartate may exhibit an asymmetric vibrational oscillation about its two C—O bonds, where one bond may be longer, shorter, or of equal length with respect to the other (**Figure 6**). In this dissertation, the longer C—O bond is denoted as r[C—O] and its respective χ_2 torsional angle is denoted normally. On the other hand, the shorter C—O bond is denoted as R[C—O*] and its respective χ_2 torsional angle is denoted as χ_2*.

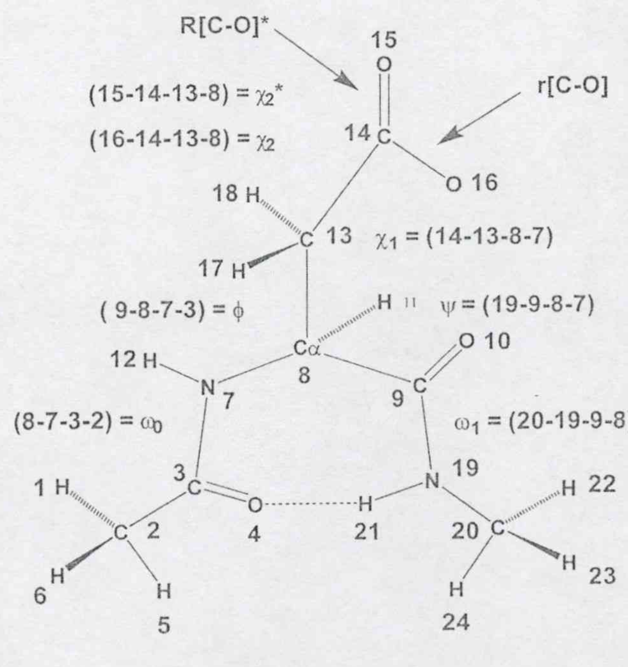

Figure 6 Definitions of atomic numbering and torsional angles for N-acetyl-*L*-aspartate-N'-methylamide.

It is interesting to explore the protonation preference for the aspartate anion. Depending on where on the carboxylate sidechain it is protonated, an aspartate anion will transform into the *endo* or *exo* form of its aspartic acid sidechain counterpart. At the end, there could be two *endo* and two *exo* protonation location

(**Figure 7**). Hence in this dissertation, a protonation model is proposed for **N**-acetyl-*L*-aspartate-**N'**-methylamide where the H atom will protonate each conformer of the aspartate residue at a maximum of four locations. The two possible *endo* protonated forms {denoted by **[2]** and **[3]** in **Figure 7**} differ from one another by a χ_2 rotation of 180°. Likewise, the two possible *exo* protonated forms {denoted by **[1]** and **[4]** in **Figure 7**} differ from one another also by a χ_2 rotation of 180°. The process can also be expressed in terms of deprotonation of the aspartic acid sidechain.

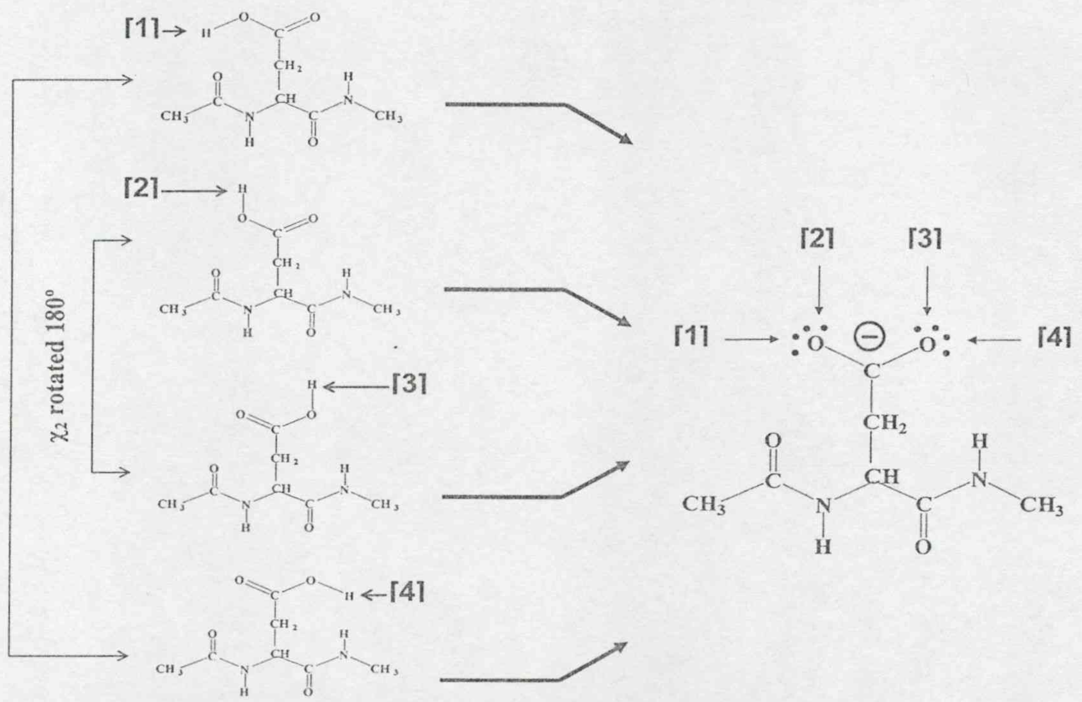

Figure 7 Deprotonation choices for **N**-acetyl-*L*-aspartic acid-**N'**-methylamide: [1] and [4] depicts the protonated *exo* form while [2] and [3] depicts the protonated *endo* form. The two *exo* forms (and the two *endo* forms) differ from one another by having their χ_2 torsional angles rotated by 180°.

In the present dissertation, all possible sidechain and backbone conformers that may exist for the aspartic acid residue, N-acetyl-*L*-aspartic acid N'-methylamide, in both its *endo* and *exo* forms together with those of N-acetyl-*L*-aspartate-**N'**-methylamide are reported. The sidechain carboxyl group of this particular aspartic acid residue is capable to inter- and intra-residual as well as intermolecular hydrogen bonding, characteristics that may be responsible for the peptide's many applications in biology and medicine. All computed results in this dissertation have been published previously[52-55].

2. CHOICE OF TOPIC

There are only two naturally occurring amino acids that have a carboxylic acid (or carboxylate ion) in their sidechains. Aspartic acid (or aspartate ion) is one of the two. Based upon this observation, it might be expected that aspartic acid (or aspartate ion) plays important roles in biological systems (**Figure 8**). Among others, these important biological functions include the following:

(i) The aspartate sidechain holds the Ca^{2+} ion in numerous proteins.

(ii) The adhesive motif Arg-Gly-Asp (or RGD for short) contains aspartate ion in its sequence.

(iii) Nowadays in molecular biology and medical studies, point mutation studies are frequently employed and the point mutations of the aspartate sidechain to another amino acid have been shown to affect signal transduction as well as translation of proteins.

(iv) In studies that involve aging, it has been shown that K and Mg salts of aspartic acid intake allow rats to survive longer by as much as 30%.

For the understanding of these studies, and numerous other biologically important phenomena, it became necessary to carry out a rigorous study on the aspartic acid residue and its sidechain deprotonated conjugate base, the aspartate ion.

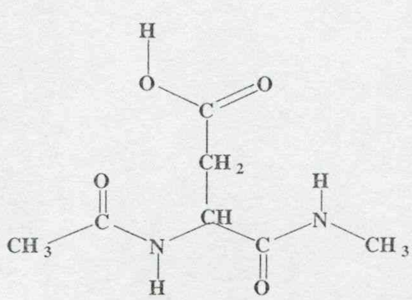

Endo Asp

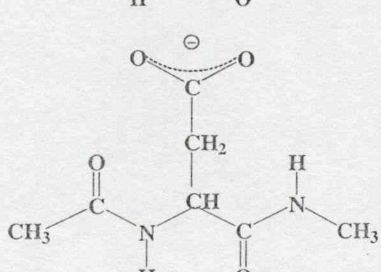

Asp(-)

Figure 8 Schematic representation of the title compounds.

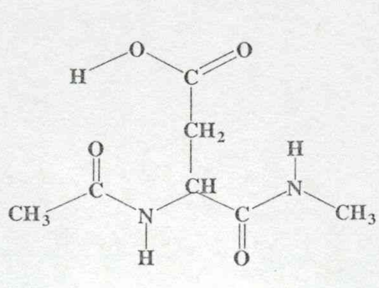

Exdo Asp

3. AIM OF STUDY

Deprotonation of an acid is normally regarded as a relatively simple process. However, if deprotonation happens in a folded protein, one may not know in advance whether the departure of a proton will or will not influence the folded structure substantially.

The present study aimed to provide, at least putatively, answers to such questions concerning factors that affect folding structures. The geometric preference of the aspartic acid residue, and that of the aspartate residue, may directly affect the function of a protein. For example, if the aspartic acid residue changes its backbone from one region to another, then the shape of an aspartic acid-containing (or aspartate-containing) protein may be altered. The three-dimensional shape of a protein essentially governs its main function. For this reason, it was necessary to study the full conformational space of both the aspartic acid and that of its deprotonated conjugate base, the aspartate ion.

Traditionally it is convenient to think in terms of vertical proton affinity (VPA) and adiabatic proton affinity (APA). **Figure 9** shows schematically their relationship.

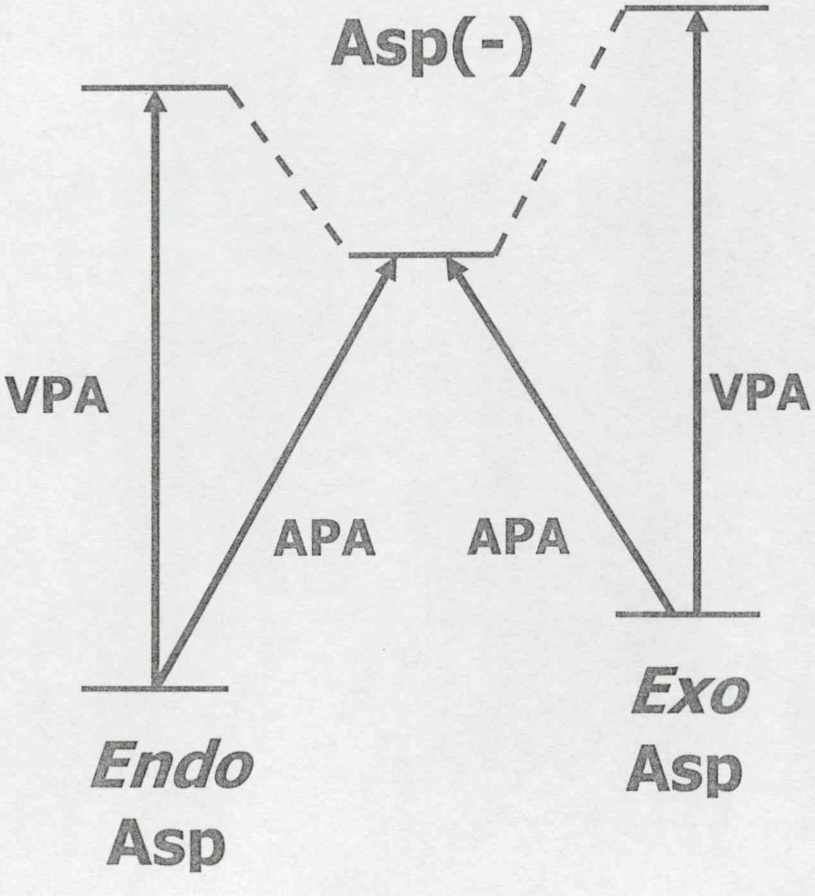

Figure 9 Schematic representation of the vertical and adiabatic deprotonation energies (or proton affinities).

4. METHODS

4.1 Gaussian Computations

Using GAUSSIAN 94[56] and GAUSSIAN 98[57], *ab initio* calculations were performed on all possible conformers for both *endo* and *exo* forms of N-acetyl-*L*-aspartic acid **N'**-methylamide as well as for **N**-acetyl-*L*-aspartate-**N'**-methylamide. Specifically, these calculations were carried out on all backbone conformations (γ_L, β_L, δ_L, α_L, ε_L, γ_D, δ_D, α_D, and ε_D) of the aspartic acid as well as the aspartate residue. The sidechain geometry of N-acetyl-*L*-aspartic acid **N'**-methylamide can be related to that of propionic acid, CH_3-CH_2-COOH. Here, the carboxyl group can be in the *endo* or *exo* form, where χ_3 is 180° or 0°, respectively (**Figure 2**).

Likewise, CH_3-CH_2-COO^- was used to mimic the geometric characteristics of the aspartate sidechain. Since there could be $3^2 = 9$ structures from backbone conformations (γ_L, β_L, δ_L, α_L, ε_L, γ_D, δ_D, α_D, ε_D) and that there could be $3^2 = 9$ sidechain orientations (χ_1, χ_2), there could exist a maximum of 9 x 9 = 81 possible conformers for the aspartate residue at each level of theory. In this dissertation, only the B3LYP/6-31G(d) results will be reported for the optimized geometries. As a result, 9 x 9 = 81 initial conformers were calculated at the RHF/3-21G level of theory for each of the three species studied. Subsequently, all stable conformers found at RHF/3-21G were subjected to re-optimizations at the RHF/6-31G(d) level of theory. Likewise, all stable conformers found at the RHF/6-31G(d) level were subsequently subjected to geometry optimization at the B3LYP/6-31G(d) level of theory. All calculations were performed at tight geometry settings using Berny Optimization: FOPT = (TIGHT, Z-MATRIX); which, at termination, produced critical points that had gradients of less than 1.5×10^{-5} a.u.

In addition, partially relaxed PEHS scan calculations, where E = E (χ_1, χ_2) and FOPT = (Z-MATRIX), were performed on both the *endo* and the *exo* forms of N-acetyl-*L*-aspartic acid **N'**-methylamide at RHF/3-21G. Here, setting and specifying the ϕ, ψ, and χ_3 torsional angles allow the backbone of the aspartic acid residue to be fixed to either the *endo* or the *exo* form as well as to their respective backbone conformations (γ_L, β_L, δ_L, α_L, ε_L, γ_D, δ_D, α_D, and ε_D).

Similarly, partially relaxed PEHS double-scan calculations were performed at the RHF/3-21G level of theory on the backbone conformations in which all stable conformers were found (γ_L, β_L, α_L, α_D) for **N**-acetyl-*L*-aspartate-**N'**-methylamide. These scan calculations, where E = E (χ_1, χ_2), were carried out under normal condition where (FOPT = Z-MATRIX). By setting and specifying the ϕ and ψ torsional angles, the aspartate was fixed to the specified backbone conformations. In addition, the two sidechain variables, χ_1 and χ_2, were rotated with 30.0° increments, resulting in 12 x 12 = 144 points. Consequently, all critical points generated in these scan calculations had gradients of less than 4.5 x 10^{-4} au.

4.2 Stabilization Energies

The stabilization or destabilization energy exerted by the sidechain on the backbone was calculated using the following isodesmic reactions with respect to the γ_L [4] and the β_L [5] backbones of the glycine residue:

$$\underset{\gamma_L}{CH_3\text{-}CO\text{-}(NH\text{-}CH_2\text{-}CO)\text{-}NHCH_3} + CH_3\text{-}R \rightarrow \underset{\text{any conformation}}{CH_3CO\text{-}(NH\text{-}CHR\text{-}CO)\text{-}NHCH_3} + CH_4 + \Delta E^{stabil}(\gamma_L) \qquad [4]$$

$$\underset{\beta_L}{CH_3\text{-}CO\text{-}(NH\text{-}CH_2\text{-}CO)\text{-}NHCH_3} + CH_3\text{-}R \rightarrow \underset{\text{any conformation}}{CH_3CO\text{-}(NH\text{-}CHR\text{-}CO)\text{-}NHCH_3} + CH_4 + \Delta E^{stabil}(\beta_L) \qquad [5]$$

Here, CH_3-R stands for CH_3-CH_2-COOH and CH_3CO-(NH-CHR-CO)-$NHCH_3$ stands for **N**-acetyl-*L*-aspartic acid **N'**-methylamide. Likewise, CH_3-R can also stand for CH_3-CH_2-COO^-; and CH_3CO-(NH-CHR-CO)-$NHCH_3$ stands for N-acetyl-*L*-aspartic acid N'-methylamide. **Table 1** shows the energies for each component of the isodesmic reaction.

Table 1

Optimized energies (hartree) of the various components in the isodesmic reactions used in the calculation of stabilization energy values at the B3LYP/6-31G(d) level of theory.

	CH_3-CO-(NH-CH_2-CO)-$NHCH_3$ (γ_L)	CH_3-CO-(NH-CH_2-CO)-$NHCH_3$ (β_L)	CH_3-CH_2-COOH	CH_3-CH_2-COO^-	CH_4
Energy (hartree)	-456.537515	-456.5357122	-268.3966238	-267.815181	-40.518383

Figure 10 provides an example of the stabilization energy calculation for the *endo* form of the aspartic acid residue at the B3LYP/6-31G(d) level of theory. Likewise, the stabilization energies of all conformers found for both the *exo* form of the aspartic acid residue as well as the aspartate residue were performed as illustrated in **Figure 10**.

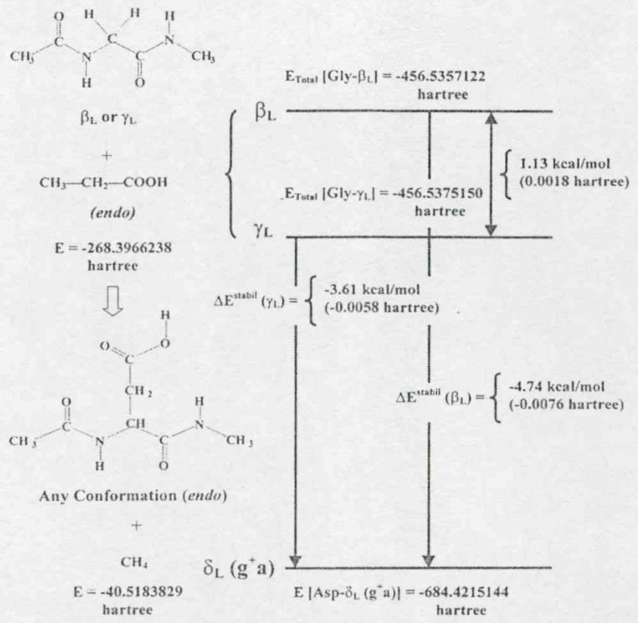

Figure 10 Definition of stabilization energies of the *endo* form of **N**-acetyl-*L*-aspartic acid **N'**-methylamide with respect to the γ_L or β_L conformer of **N**-acetyl glycine **N'** methylamide.

Note that the two stabilization values (from equations [4] and [5]) are shifted with respect to each other by 1.13 kcal/mol at B3LYP/6-31G(d). This shift in stabilization energy [6] corresponds to the difference in relative energies between the β_L and γ_L backbone conformation for the glycine diamide:

$$\text{B3LYP/6-31G(d)} \qquad \Delta E^{stabil}(\beta_L) - \Delta E^{stabil}(\gamma_L) = 1.13 \text{ kcal/mol} \qquad [6]$$

In the past, ΔE^{stabil} (γ_L) was favoured in stabilization energy calculations, as the global minimum for most of the single amino acid diamides in the gas phase is usually located at the γ_L backbone. Interestingly, when fully extended, the β_L conformation is highly symmetrical and it represents a unique structure on the Ramachandran map. As a result, ΔE^{stabil} (β_L) is becoming a more accepted parameter for stabilization energy calculations[58-60].

5. RESULTS AND DISCUSSION

5.1 Aspartic Acid

5.1.1 Endo Form of Aspartic Acid

5.1.1.1 Molecular Geometry of the Endo Form of Aspartic Acid

Initially, the sidechain PESs, E = E (χ_1, χ_2) were generated for each one of the nine backbone conformations (γ_L, β_L δ_L, α_L, γ_D, δ_D, α_D, ε_D). The nine sidechain PESs, shown in landscape representation (**Figure 11**) and contour representation (**Figure 12**), exhibited numerous minima.

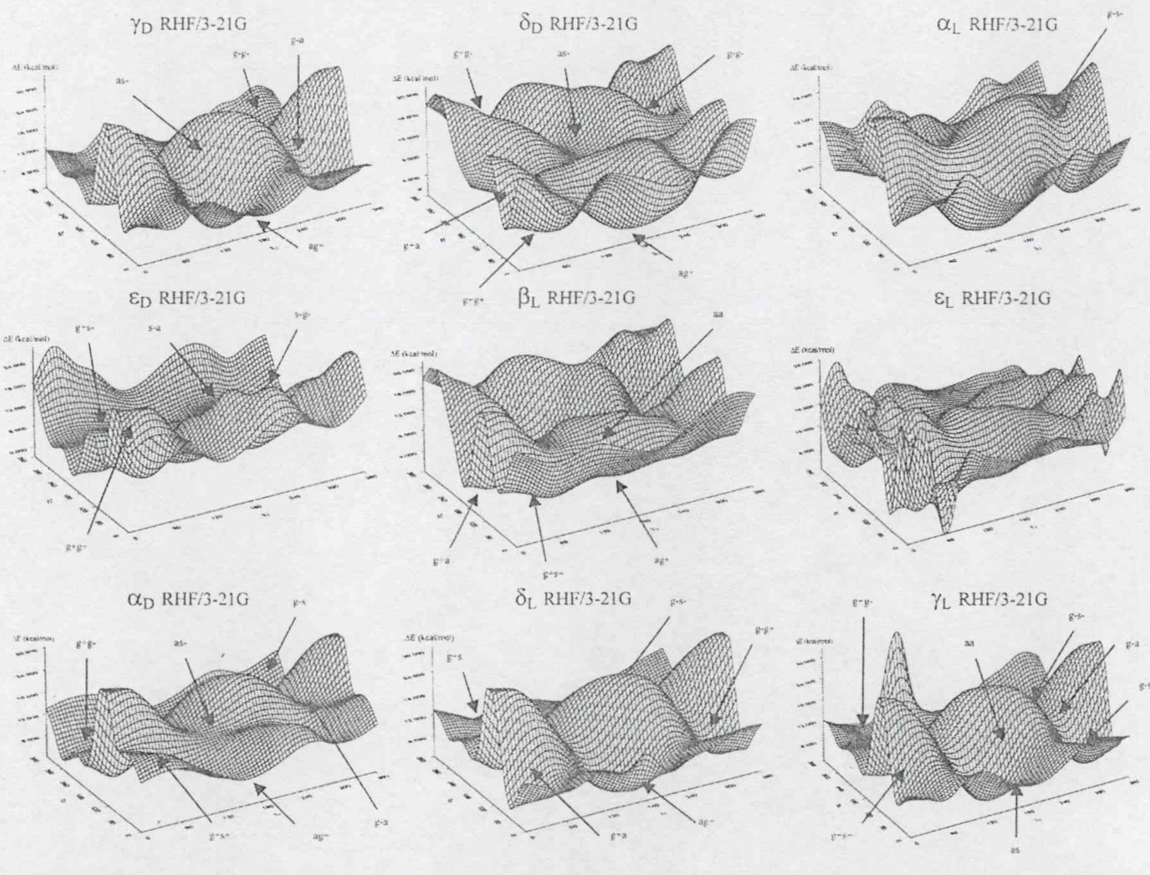

Figure 11 Landscape representation of the nine sidechain conformational PEHSs, E = E (χ_1, χ_2) associated with each one of the nine backbone conformations for the *endo* form of the aspartic acid residue. Torsional angles χ_1 and χ_2 are given in degrees from 0° to 360°.

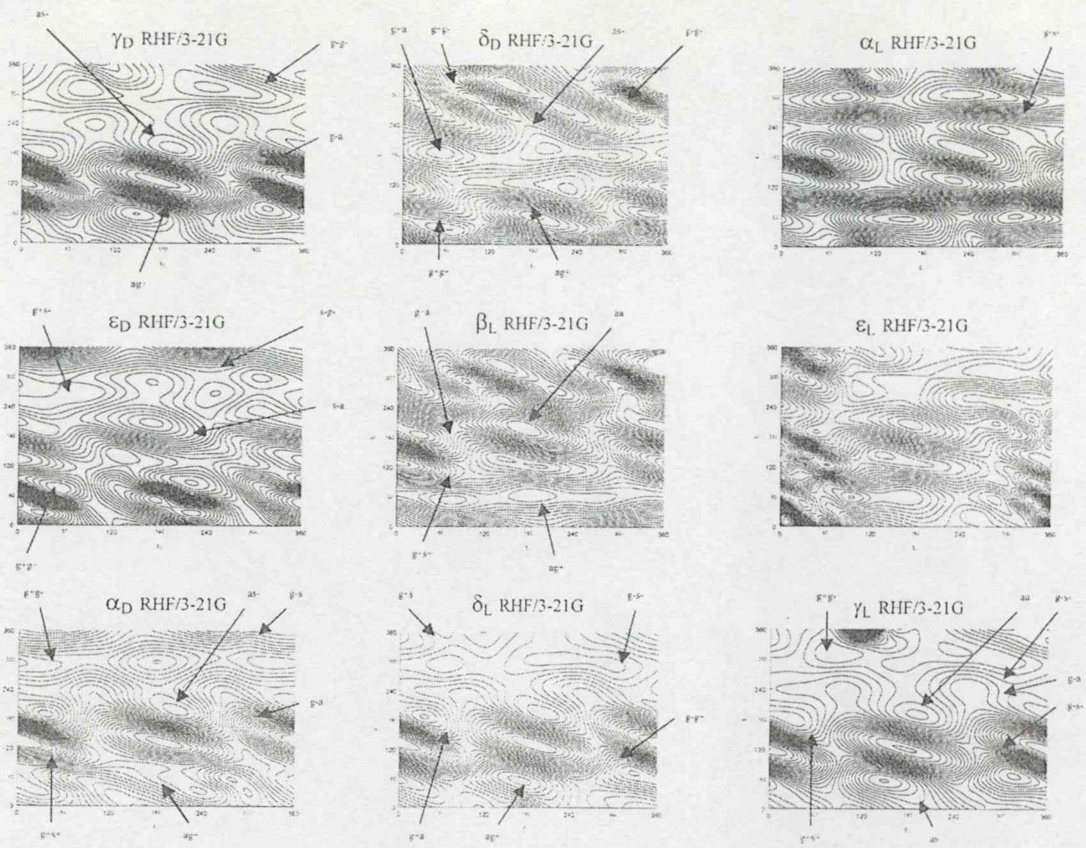

Figure 12 Contour representation of the nine sidechain conformational PEHSs, E = E (χ_1, χ_2) associated with each one of the nine backbone conformations for the *endo* form of the aspartic acid residue. Torsional angles χ_1 and χ_2 are given in degrees from 0° to 360°.

When these apparent minima were optimized only some of them turned out to be true minima. Such apparent discrepancies may well be expected since the torsional angles ϕ and ψ were frozen. Furthermore, it has to be recognized that in a double-scan such as E = E (χ_1, χ_2), grid points are optimized at fixed $\chi_1$and χ_2 values. Consequently, these semi-rigid optimizations do not precisely correspond to optimized structures. Thus, any minimum appearing on a surface may not be a minimum on the hypersurface. Sometimes, such "false" minima may represent higher order critical points such as transition structures. Also, a minimum appearing on a surface may be shifted somewhat to a regional neighbour. The position of the minima which were located successfully (i.e. "converged") during the optimization process are also shown by arrows in **Figures 11** and **Figure 12**. **Table 2** summarizes the optimized dihedral angles and energies of the 37 optimized conformers out of a grand total of 81 expected structures.

Table 2

Optimized conformers of N-acetyl-*L*-aspartic acid N'-methylamide in its *endo* form for all its stable backbone (γ_L, β_L, δ_L, α_L, γ_D, δ_D, α_D, and ε_D) conformations computed at the B3LYP/6-31G(d) level of theory. Shown here are the optimized torsional angles, computed energy values, relative energies, and stabilization energies.

Final Conform.	Optimized Parameters									
BB [$\chi_1 \chi_2$]	ϕ	ψ	ω_0	ω_1	χ_1	χ_2	E_{min} (hartree)	ΔE (kcal/mol)	ΔE^{stabil} (kcal) γ_L	ΔE^{stabil} (kcal) β_L
					γ_L **Backbone Conformation**					
γ_L [g^+s^+]	-82.63	69.39	-179.63	-176.47	58.85	144.19	-684.4260542	0.000	-6.4623	-7.5936
γ_L [g^+g^-]	-83.22	70.88	-179.64	-176.59	67.76	-41.53	-684.4210847	3.118	-3.3439	-4.4751
γ_L [a s]	-83.13	69.16	-178.12	-177.73	-176.54	27.91	-684.4178720	5.134	-1.3279	-2.4591
γ_L [a a]	-82.80	71.63	-179.13	-177.93	-169.19	-163.60	-684.4199177	3.851	-2.6116	-3.7428
γ_L [g^-s^+]	-83.30	71.37	-173.51	-176.48	-55.28	90.31	-684.4190950	4.367	-2.0953	-3.2266
γ_L [g^- a]	-84.30	66.13	-173.78	-177.94	-72.14	157.14	-684.4189046	4.486	-1.9758	-3.1071
γ_L [g^-s^-]	-83.95	72.82	-170.48	-175.81	-45.07	-119.39	-684.4217674	2.690	-3.7723	-4.9035
					β_L **Backbone Conformation**					
β_L [g^+s^+]	-170.22	150.84	-169.30	175.92	58.82	107.24	-684.4154168	6.675	0.2128	-0.9185
β_L [g^+ a] [a,b]	-157.77	-177.22	173.48	-179.57	66.22	-171.49	-684.4153786	6.699	0.2368	-0.8945
β_L [a g^+]	-164.40	162.84	177.73	177.71	-173.28	32.25	-684.4184974	4.742	-1.7203	-2.8516
β_L [a a]	-163.51	167.73	175.07	178.61	-161.48	173.27	-684.4240236	1.274	-5.1881	-6.3193
					δ_L **Backbone Conformation**					
δ_L [g^+ s]	-130.53	32.86	-170.39	176.65	69.12	-26.01	-684.4164380	6.034	-0.4280	-1.5593
δ_L [g^+ a] [a,b]	-130.74	30.06	-170.27	177.91	60.44	162.32	-684.4215144	2.849	-3.6135	-4.7448
δ_L [a g^+]	-135.53	34.83	-170.11	175.22	-172.91	37.96	-684.4130412	8.166	1.7035	0.5722
δ_L [g^-g^+]	-135.08	25.11	-164.18	174.86	-67.72	82.47	-684.4133097	7.997	1.5350	0.4037
δ_L [g^-s^-]	-133.61	22.39	-161.57	175.51	-56.89	-98.79	-684.4155795	6.573	0.1107	-1.0206
					α_L **Backbone Conformation**					
α_L [g^-s^-] [a,b]	-81.20	-13.35	-164.10	176.83	-55.35	-119.10	-684.4153827	6.696	0.2342	-0.8971
					γ_D **Backbone Conformation**					
γ_D [a g^+]	73.01	-53.01	175.99	-176.30	-170.77	65.87	-684.4128945	8.258	1.7956	0.6643
γ_D [a s^-] [a,b]	74.54	-65.87	178.99	177.75	-155.29	-145.77	-684.4128963	8.257	1.7944	0.6632
γ_D [g^- a]	73.63	-49.71	168.25	-178.12	-64.89	179.52	-684.4181554	4.957	-1.5057	-2.6370
γ_D [g^-g^-]	72.81	-53.52	172.24	-178.73	-59.41	-37.44	-684.4146876	7.133	0.6704	-0.4609
					δ_D **Backbone Conformation**					
δ_D [g^+g^+] [a,b]	-155.89	-38.80	171.16	-175.78	43.03	44.58	-684.4069299	12.001	5.5384	4.4071
δ_D [g^+ a] [a,b]	-156.90	-48.59	174.77	-176.77	54.07	-168.35	-684.4146306	7.168	0.7061	-0.4251
δ_D [g^+g^-]	-164.26	-45.65	176.01	-175.35	67.67	-35.23	-684.4075771	11.595	5.1323	4.0010
δ_D [a g^+]	-169.53	-39.89	168.72	-171.72	178.57	65.29	-684.4067348	12.123	5.6608	4.5296
δ_D [a s^-]	-173.40	-36.11	167.19	-172.40	-172.30	-117.79	-684.4058219	12.696	6.2337	5.1024
δ_D [g^-g^-] [a,b]	-144.09	-61.07	178.05	-176.94	-61.73	-79.40	-684.4052097	13.080	6.6178	5.4866
					α_D **Backbone Conformation**					
α_D [g^+s^+]	58.20	35.63	161.69	-175.78	42.53	102.03	-684.4070563	11.921	5.4591	4.3278
α_D [g^+g^-]	59.50	29.35	164.08	-176.20	55.10	-81.81	-684.4040903	13.783	7.3203	6.1890
α_D [a g^+]	65.49	31.81	168.69	-176.91	-167.04	37.82	-684.4097827	10.211	3.7482	2.6170
α_D [a s^-]	66.30	32.61	169.86	-177.78	-157.47	-149.78	-684.4122840	8.641	2.1787	1.0474
α_D [g^- s]	66.36	28.71	166.07	-177.25	-63.19	-18.36	-684.4119363	8.859	2.3968	1.2656
α_D [g^- a]	66.01	30.43	164.61	-177.19	-64.43	-176.83	-684.4166005	5.932	-0.5300	-1.6613
					ε_D **Backbone Conformation**					
ε_D [g^+g^+]	53.92	-123.45	-176.20	177.24	51.08	89.57	-684.4079873	11.337	4.8749	3.7436
ε_D [g^+s^-]	57.16	-134.18	-164.86	179.14	69.41	-103.68	-684.4113997	9.196	2.7336	1.6023
ε_D [s^- a]	66.93	-178.82	-158.02	-175.88	-149.86	160.48	-684.4142905	7.382	0.9196	-0.2117
ε_D [s^-g^-]	64.41	-167.41	-160.60	-175.48	-135.38	-50.94	-684.4076898	11.524	5.0616	3.9303

[a] After 200 iterations under (TIGHT) at B3LYP/6-31G(d), the force has converged, but the displacement did not converge completely.

[b] This result was obtained from a regular optimization fully converged at B3LYP/6-31G(d).

Table 2 reveals that along χ_2, when the planar COOH moiety was rotated against the tetrahedral β-carbon, sometimes there existed a noticeable shift in the torsional angle away from the typical g^+ value (60°) or from the typical g^- value (-60°) towards the *anti* orientation (+180° or -180° respectively). Such values that fell within the range of +90° and +150° (i.e. +120° ± 30°) were labeled as *syn*$^+$ (or s^+) indicating that the OH oxygen of the carboxyl moiety was in *syn* orientation with respect to the proton at about +120°. Similarly, values that fell within the range of -90° and -150° (i.e. -120° ± 30°) were labeled as *syn*$^-$ (or s^-) indicating that the OH oxygen of the carboxyl moiety was in *syn* orientation with the proton at about -120°.

Figure 13 illustrates the various hydrogen bonds that may exist in the *endo* form of **N**-acetyl-*L*-aspartic acid **N'**-methylamide.

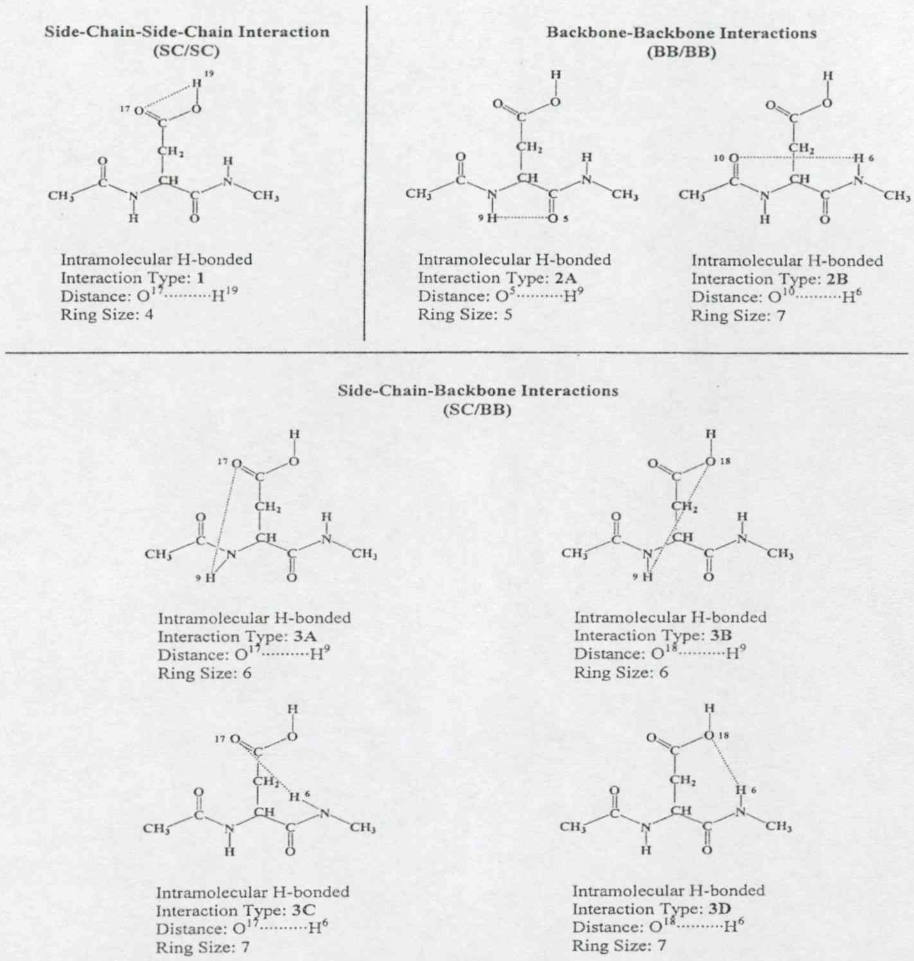

Figure 13 Classification of the types of internal hydrogen bonding for the *endo* form of **N**-acetyl-*L*-aspartic acid **N'**-methylamide.

The corresponding distances for these hydrogen bond interactions are tabulated on **Table 3**.

Table 3

The relative distances of intramolecular hydrogen bonds of **N**-acetyl-*L*-aspartic acid **N**'-methylamide in its *endo* form for all its stable backbone (γ_L, β_L, δ_L, α_L, γ_D, δ_D, α_D, and ε_D) conformations computed at the B3LYP/6-31G(d) level of theory. No conformers were found for the ε_L backbone and hence no hydrogen bond distances for the ε_L backbone could be tabulated.

Final Conform.	Interaction Type			Distance (Å) *						
BB [χ_1 χ_2]	SC/SC	BB/BB	SC/BB	O17-H19	H9-O17	H9-O18	H9-O5	H6-O10	H6-O17	H6-O18
γ_L Backbone Conformation										
γ_L [g^+s^+]	1	2B	3A	2.274	2.056	3.924	3.565	2.030	4.945	5.833
γ_L [g^+g^-]	1	2B	3B	2.276	4.026	2.109	3.554	2.053	5.858	4.893
γ_L [a s]	1	2B	-	2.282	4.911	4.701	3.632	2.044	5.761	4.260
γ_L [a a]	1	2B	-	2.283	4.774	4.895	3.588	2.066	4.277	5.797
γ_L [g^-s^+]	1	2B	-	2.281	3.778	2.419	3.747	1.986	5.506	5.566
γ_L [g^- a]	1	2B	-	2.280	3.638	3.859	3.720	2.004	4.922	6.155
γ_L [g^-s^-]	1	2B	3A	2.275	2.097	3.807	3.834	1.952	5.416	5.873
β_L Backbone Conformation										
β_L [g^+s^+]	1	2A	-	2.281	2.906	4.064	2.261	4.891	5.233	4.343
β_L [g^+ a] [a,b]	1	2A	-	2.282	3.161	4.713	2.117	5.099	3.719	4.322
β_L [a g^+]	1	2A	3D	2.266	5.406	4.935	2.120	4.999	3.587	2.196
β_L [a a]	1	2A	3C	2.270	4.988	5.509	2.074	5.040	1.984	3.864
δ_L Backbone Conformation										
δ_L [g^+ s]	1	-	3B	2.270	4.129	2.215	3.832	3.543	5.674	4.065
δ_L [g^+ a] [a,b]	1	-	3A	2.275	2.179	4.031	3.850	3.588	4.038	5.649
δ_L [a g^+]	1	-	-	2.282	5.107	4.838	3.784	3.617	5.887	4.899
δ_L [g^-g^+]	1	-	-	2.271	4.514	3.111	3.921	3.649	5.828	5.281
δ_L [g^-s^-]	1	-	-	2.286	2.950	4.333	3.978	3.641	5.245	5.773
α_L Backbone Conformation										
α_L [g^-s^-] [a,b]	1	-	3A	2.281	2.121	3.843	4.397	3.014	4.822	5.831
γ_D Backbone Conformation										
γ_D [a g^+]	1	2B	-	2.288	5.505	4.611	3.941	1.927	4.230	4.972
γ_D [a s^-] [a,b]	1	2B	-	2.282	4.558	5.581	3.754	1.957	4.856	4.483
γ_D [g^- a]	1	2B	-	2.282	2.787	4.517	4.096	1.873	4.856	5.279
γ_D [g^-g^-]	1	2B	-	2.271	4.307	3.193	3.992	1.894	4.856	5.111
δ_D Backbone Conformation										
δ_D [g^+g^+] [a,b]	1	-	3D	2.250	4.467	3.351	3.623	4.853	4.126	2.078
δ_D [g^+ a] [a,b]	1	-	3C	2.265	3.075	4.664	3.624	4.874	1.961	3.961
δ_D [g^+g^-]	1	-	3D	2.247	4.876	3.084	3.608	4.760	3.630	2.151
δ_D [a g^+]	1	-	-	2.288	5.341	5.097	3.554	4.602	4.205	4.952
δ_D [a s^-]	1	-	-	2.282	5.154	5.363	3.573	4.532	5.105	4.349
δ_D [g^-g^-] [a,b]	1	-	-	2.303	4.032	4.740	3.570	5.004	4.531	5.101
α_D Backbone Conformation										
α_D [g^+s^+]	1	-	-	2.283	3.329	4.602	4.456	2.800	5.109	5.092
α_D [g^+g^-]	1	-	-	2.268	4.793	3.475	4.453	2.713	5.081	4.996
α_D [a g^+]	1	-	-	2.274	5.453	4.439	4.428	3.070	5.888	4.999
α_D [a s^-]	1	-	-	2.278	4.445	5.421	4.424	3.143	5.063	5.913
α_D [g^- s]	1	-	-	2.261	4.199	2.721	4.438	2.974	6.132	5.031
α_D [g^- a]	1	-	-	2.275	2.528	4.295	4.437	2.993	5.048	6.198
ε_D Backbone Conformation										
ε_D [g^+g^+]	1	-	3D	2.293	4.062	4.881	3.321	2.932	3.782	2.030
ε_D [g^+s^-]	1	-	3C	2.279	5.051	4.461	2.990	3.281	1.942	3.740
ε_D [s^- a]	1	-	3C	2.268	4.856	5.512	2.783	4.718	1.966	3.800
ε_D [s^-g^-]	1	-	3D	2.273	5.203	4.879	2.763	4.444	3.960	2.025

[a] After 200 iterations under (TIGHT) at B3LYP/6-31G(d), only the force has converged, but the displacement did not converge completely.

[b] This result was obtained from a regular optimization fully converged at B3LYP/6-31G(d).

* Atomic numbering is given in **Figure 2** (left).

As shown in **Figure 13**, there exists one sidechain-sidechain (SC/SC) hydrogen bond interaction that existed in all stable conformers found for the aspartic acid residue. Since all stable conformers possess this SC/SC interaction, it is plausible that this type of hydrogen bonding serves to stabilize the general structure of the amino acid in the *endo* orientation. In addition to the SC/SC interaction, there exist two backbone-backbone (BB/BB) interactions and four sidechain-backbone (SC/BB) interactions. The BB/BB interaction can be viewed as an internal stabilizing factor that allows fundamental stability for the aspartic acid residue while at the same time allowing the sidechain to participate in external interactions with other substrates. On the other hand, the SC/BB interaction can induce even greater internal stability to the aspartic acid residue than the SC/SC interaction. An example to illustrate this phenomenon exists in the $g^- s^-$ of the α_L conformation. Here, type 3A of the hydrogen bond interaction seems to contribute a major stabilizing force that allows for the existence of this unlikely-found conformer at the α_L backbone. Moreover, it is worth noting that a rather weak H········ Ninteraction (distance = 2.2758 Å, not included in **Table 3**) seems to exist for the α_L conformer, shown in **Figure 14**.

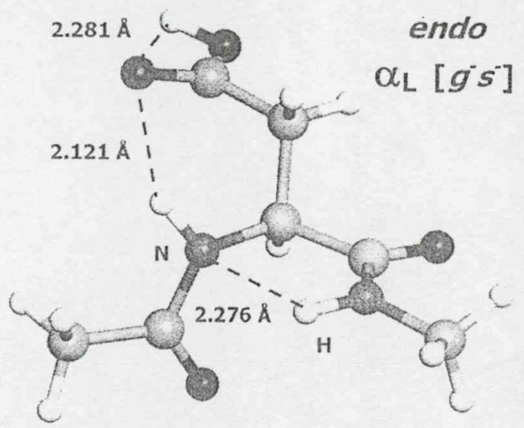

Figure 14 A new type of backbone-backbone (—CON—H····· NHCO—) hydrogen bonding observed in the case of the α_L [$g^- s^-$] conformation at H····· Ndistance of 2.276 Å in addition to regular hydrogen bonds for the *endo* form of the aspartic acid residue.

Such unusual interaction, which could be categorized as a BB/BB interaction (although not shown in **Figure 13**), may also be a contributing reason of the existence of the α_L conformer. A correlating trend between hydrogen bond distance and ring size (RS) is shown in **Figure 15**. Here, it is apparent that the shorter the hydrogen bond distance, the greater the RS. The overall correlation equation shows a least square value of $R^2 = 0.8443$, showing that such trend is rational and realistic. Interestingly, it was also observed that in some cases, the ω_0 torsional angle of some stable conformers (such as those found in the α_D conformation) have deviated from the ideal value of 180°. Such an example can be found at the δ_L [$g^- s^-$], α_L [$g^- s^-$], α_D [$g^+ s^+$], and ε_D [$s^- a$] conformers.

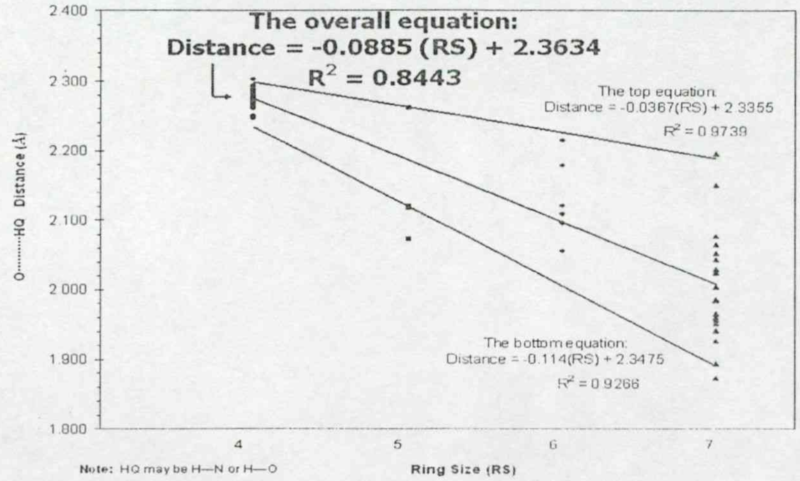

Figure 15 A trend showing the interrelation between hydrogen-bonded distance and ring size (RS) of internal hydrogen bonds for the *endo* form of **N**-acetyl-*L*-aspartic acid **N**'-methylamide.

One possible reason for such rather strange occurrences could be the existence of hydrogen bond interactions that act as stabilizing forces for these conformers. For instance, the δ_L [$g^- s^-$] conformer has a potential hydrogen bond interaction (2.950 Å) between H^{19} and O^{17}, as shown in **Table 3**. Although this particular interaction, a potential SC/BB, was not categorized as a hydrogen bond (our definition for a hydrogen bond interaction of **N**-acetyl-*L*-aspartic acid **N**'-methylamide in its *endo* form is 2.300 Å), it shows that it has a slight inclination in forming a potential interaction that can act as a stabilizing factor for the conformer. Likewise, other conformers mentioned above which have deviated ω_0 angles all have at least one other type of potential hydrogen bonding that can act as important stabilizing forces for the conformer itself. In addition, this may suggest that as a particular conformer seeks to stabilize its sidechain with its backbone, it may be willing to rotate one of its adjacent peptide bonds away from coplanarity. This mechanism is one of compromise, where a conformer may change, for example, its ω_0 torsional angle in order to form a weak hydrogen bond that may stabilize itself even to a greater extent. Such an observation may deem important when considering the aspartic acid residue's role in the RGD tripeptide. If it is true that the aspartic acid is willing to offset its torsional angles in order to achieve greater stability, then it can also do so in concordance with other members of the RGD moiety, namely arginine and glycine, for an overall stability of the tripeptide. In this case, it is very likely that significant BB/BB and SC/BB interactions would be involved in the overall stability of the RGD. Hence, it is not surprising to recognize from **Table 3** that aside from the SC/SC interaction there are two additional hydrogen bond types, namely BB/BB and SC/BB, which help to stabilize the conformers of the γ_L and β_L backbones. Interestingly, these two backbones are traditionally known as being the more stabilized conformations, where most of the stable conformers of an amino acid would most likely be found. Both BB/BB and SC/BB interactions allow the aspartic acid residue to achieve internal stabilization while acting as stabilizing forces for the other members of the RGD. The study of SC/BB and BB/BB interactions in N-acetyl-*L*-aspartic acid N'-methylamide may deem significant as these interactions may be present not only in the internal stabilization within the RGD but also in the external stability of the tripeptide during its binding to a foreign substrate. Since substrate binding is greatly affected by the 3D steric arrangement of molecules, it is then logical to study the stabilizing interactions within the molecules themselves. In turn, this will allow for more in-depth understanding of what brings about the different conformations for a particular substrate-binding assay.

5.1.1.2 Molecular Energetics of the Endo Form of Aspartic Acid

Figure 11 in reference 53, various stabilization energies, with respect to either β_L or γ_L of the glycine residue, are shown in a bar-graph format (Figure 11 of J. Phys. Chem A[53]) The difference in stabilization energy, ΔE^{stabil} with respect to β_L and with respect to γ_L is constant (1.13 kcal/mol), as shown in **Figure 10.**

Consequently, it is enough to discuss only one set of the stabilization energy data. Here, the values with respect to the β_L glycine residue showing at the right hand side of Figure 11[53] will be discussed. One can observe that the L substituted conformation (i.e. α_L, β_L, δ_L, γ_L) of the aspartic acid residue is more stable than its D substituted form (i.e. α_D,γ_D, δ_D, ε_D). As illustrated in Figure 11[53], most of the L conformers are stabilized. This is shown by the fact that the L subscripted conformers for N-acetyl-*L*-aspartic acid N'-methylamide either have great negative values or small positive values for their stabilization energies. This trend is observed in the γ_L, β_L δ_L and α_L backbones for the aspartic acid residue. On the other hand, most conformers found for the D subscripted form of the aspartic acid residue are in general de-stabilized. Again, shown in Figure 11[53], the D-subscripted conformers have either great positive values or small negative values for their stabilization energies. This trend exists in the α_D, γ_D, δ_D and ε_D backbones for the aspartic acid residue. An analogous trend is also shown in the stabilization energy values calculated with respect to γ_L, at the left hand side of Figure 11[53].

5.1.2 Exo Form of Aspartic Acid

5.1.2.1 Molecular Geometry of the Exo Form of Aspartic Acid

The sidechain PESs, E = E (χ_1, χ_2), were first generated for each one of the nine backbone conformations (γ_L, β_L δ_L, α_L, γ_D, δ_D, α_D, ε_D) of N-acetyl-*L*-aspartic acid N'-methylamide. These PESs revealed numerous minima, shown in landscape representation (**Figure 16**) and contour representation (**Figure 17**).

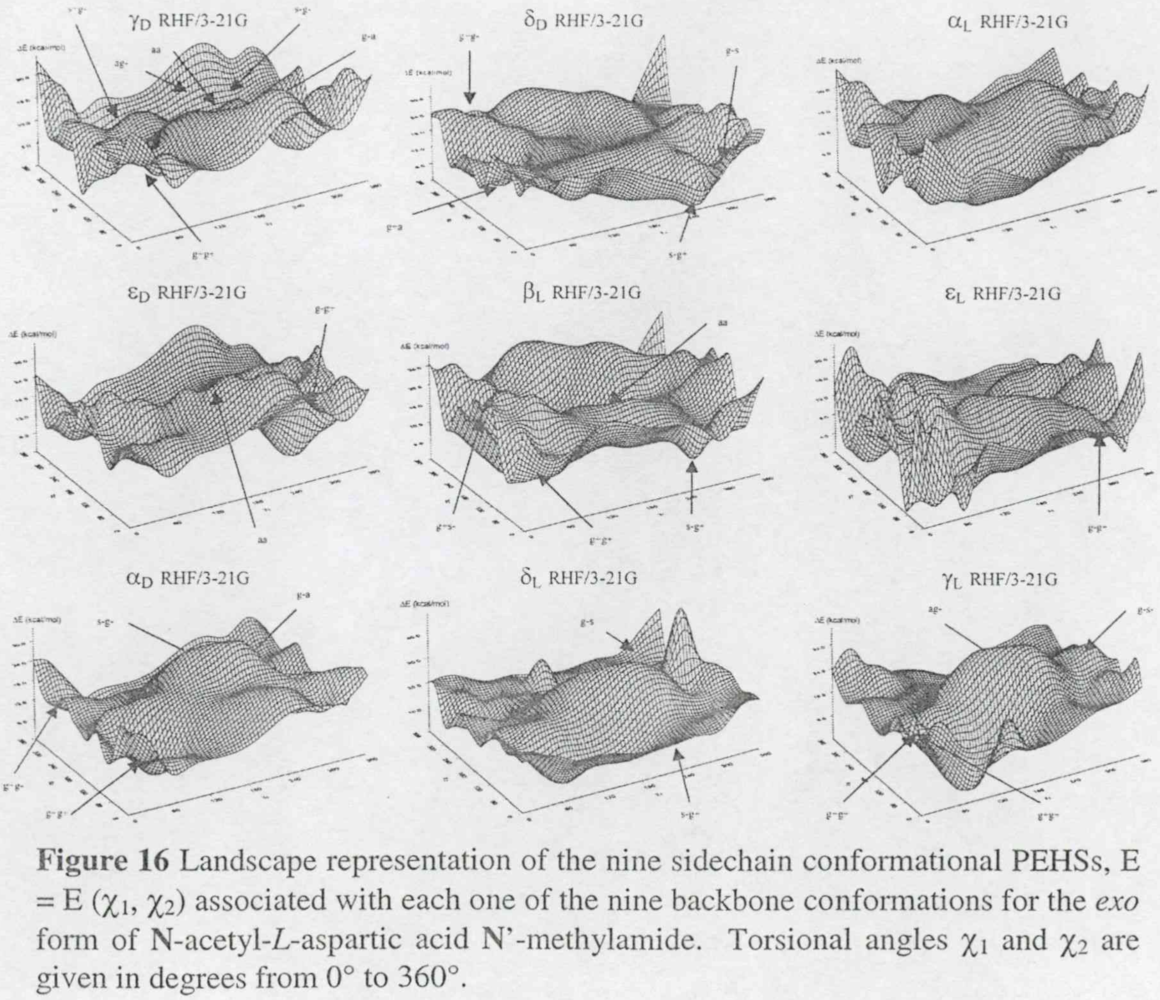

Figure 16 Landscape representation of the nine sidechain conformational PEHSs, E = E (χ_1, χ_2) associated with each one of the nine backbone conformations for the *exo* form of N-acetyl-*L*-aspartic acid N'-methylamide. Torsional angles χ_1 and χ_2 are given in degrees from 0° to 360°.

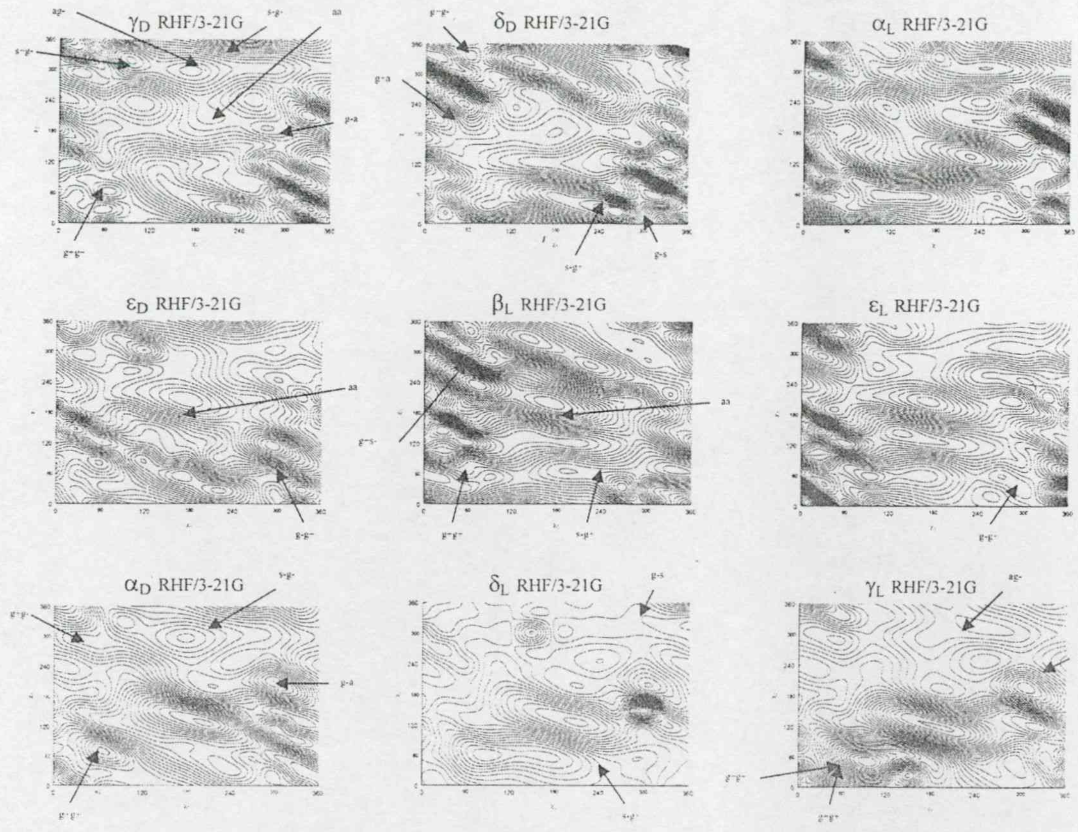

Figure 17 Contour representation of the nine sidechain conformational PEHSs, E = E (χ_1, χ_2) associated with each one of the nine backbone conformations for the *exo* form of **N**-acetyl-*L*-aspartic acid **N**'-methylamide. Torsional angles χ_1 and χ_2 are given in degrees from 0° to 360°.

However, subsequent optimizations on these apparent minima revealed that only some were true minima. Since the torsional angles ϕ and ψ were frozen, such discrepancies may well be expected. In addition, in a double-scan such as E = E (χ_1, χ_2), grid points are optimized at fixed $\chi_1$and χ_2 values. As a result, these semi-rigid optimizations do not precisely correspond to "true" optimized structures where any minimum appearing on a surface may not be a minimum on the hypersurface. Such "false" minima may represent higher order critical points such as transition structures. Also, a minimum appearing on a surface may be shifted somewhat to a regional neighbour.

The position of the minima which were located successfully (i.e. "converged") during the optimization process are also shown by arrows in **Figure 16** and **Figure 17**. All optimized dihedral angles, including the relative energies and stabilization energies, are shown in **Table 4** where only 27 out of the 81 expected structures were found.

Table 4

Optimized conformers of **N**-acetyl-*L*-aspartic acid **N'**-methylamide in its *exo* form for all its stable backbone (γ_L, β_L, δ_L, ε_L, γ_D, δ_D, α_D, and ε_D) conformations computed at the B3LYP/6-31G(d) level of theory. Shown here are the optimized torsional angles, computed energy values, relative energies, and stabilization energies.

Final Conform.	Optimized Parameters										
BB [$\chi_1\chi_2$]	ϕ	ψ	ω_0	ω_1	χ_1	χ_2	χ_3	E_{min} (hartree)	ΔE (kcal/mol)	ΔE^{stabil} (kcal) γ_L	ΔE^{stabil} (kcal) β_L
γ_L Backbone Conformation											
γ_L [g^+g^+]	-81.06	63.58	-171.12	-179.73	50.73	82.28	-13.95	-684.4265160	-0.290	-12.6619	-13.7932
γ_L [g^+g^+]	-81.91	63.80	-170.70	-179.40	50.58	82.31	-13.98	-684.4266579	-0.379	-12.7509	-13.8822
γ_L [$a\ g^-$]	-83.16	64.17	-172.10	-179.20	-165.32	-70.57	4.41	-684.4208809	3.246	-9.1258	-10.2571
γ_L [g^-s^-]	-84.07	70.53	-169.26	-176.36	-45.91	-121.27	0.59	-684.4126227	8.428	-3.9437	-5.0750
β_L Backbone Conformation											
β_L [g^+g^+] [a,b]	-156.59	-176.43	177.82	-171.12	64.56	72.14	-1.65	-684.4058456	12.681	0.3090	-0.8223
β_L [g^+s^-]	158.11	-139.74	172.36	179.88	63.71	-90.93	6.92	-684.4201077	3.731	-8.6406	-9.7719
β_L [$a\ a$]	-167.29	170.92	174.39	179.24	-159.70	167.29	-3.78	-684.4161709	6.202	-6.1702	-7.3015
β_L [s^-g^+]	-169.92	-177.45	175.01	-179.22	-130.05	74.37	-4.45	-684.4237651	1.436	-10.9357	-12.0669
δ_L Backbone Conformation											
δ_L [s^-g^+] [a,b]	-161.43	45.11	-176.35	173.71	-118.31	48.09	4.66	-684.4099383	10.113	-2.2592	-3.3905
δ_L [$g^-\ s$]	-135.40	25.16	-177.58	174.07	-67.01	-15.76	14.84	-684.4103060	9.882	-2.4900	-3.6212
ε_L Backbone Conformation											
ε_L [g^-g^+]	-94.47	149.36	160.78	177.79	-63.25	43.99	-5.09	-684.4102974	9.888	-2.4846	-3.6158
γ_D Backbone Conformation											
γ_D [g^+g^+]	64.96	-61.81	168.52	175.34	60.23	67.68	-17.12	-684.4033200	14.266	1.8938	0.7625
γ_D [s^+g^-]	79.72	-53.75	-177.65	-174.22	107.66	-75.40	6.66	-684.4073279	11.751	-0.6212	-1.7524
γ_D [$a\ a$]	74.38	-70.80	-179.62	175.29	-154.73	-154.72	4.80	-684.4035338	14.132	1.7597	0.6284
γ_D [$a\ g^-$]	70.34	-81.17	177.02	172.78	-176.52	-70.85	4.12	-684.4078146	11.446	-0.9266	-2.0579
γ_D [s^-g^-]	70.12	-28.28	167.77	-175.15	-143.16	-35.94	-3.53	-684.4144381	7.289	-5.0829	-6.2142
γ_D [$g^-\ a$]	73.63	-44.57	167.30	-177.58	-63.68	176.48	-0.54	-684.4098022	10.198	-2.1738	-3.3051
δ_D Backbone Conformation											
δ_D [$g^+\ a$] [a,b]	-160.74	-48.85	175.72	-176.93	52.48	-164.30	3.41	-684.4071457	11.865	-0.5068	-1.6381
δ_D [g^+g^-] [a,b]	-152.24	-46.34	162.79	-174.56	62.86	-42.90	-3.04	-684.4046175	13.452	1.0796	-0.0516
δ_D [s^-g^+]	-166.96	-52.06	172.53	-173.85	-121.06	55.27	4.53	-684.4070418	11.930	-0.4416	-1.5729
δ_D [$g^-\ s$] [a,b]	-135.56	-70.97	168.84	-177.26	-79.12	2.05	12.10	-684.4055002	12.898	0.5257	-0.6055
α_D Backbone Conformation											
α_D [g^+g^+]	51.02	50.87	158.65	-173.41	57.95	78.07	-13.34	-684.4118612	8.906	-3.4659	-4.5971
α_D [g^+g^-]	49.91	35.67	175.22	-176.17	42.68	-69.95	7.37	-684.3904410	22.348	9.9755	8.3442
α_D [s^-g^-]	68.57	27.90	165.45	-178.48	-147.48	-61.61	0.62	-684.4145135	7.242	-5.1302	-6.2615
α_D [$g^-\ a$]	66.58	30.54	164.64	-177.60	-64.08	-177.94	0.92	-684.4094323	10.430	-1.9417	-3.0730
ε_D Backbone Conformation											
ε_D [$a\ a$]	68.83	176.68	-157.00	-176.55	-152.00	171.32	-0.35	-684.4069842	11.967	-0.4055	-1.5368
ε_D [g^-g^+]	85.36	163.60	-152.58	178.97	-62.34	93.43	-7.44	-684.4096079	10.320	-2.0519	-3.1832

[a] After 200 iterations under (TIGHT) at B3LYP/6-31G(d), the force has converged, but the displacement did not converge completely.
[b] This result was obtained from a regular optimization fully converged at B3LYP/6-31G(d).

When examining the optimized values in **Table 4**, it is shown that when the planar —COOH moiety was rotated against the tetrahedral β-carbon (χ_2), sometimes there exist noticeable shifts in the torsional angle away from the typical g^+ value (60°) or from the typical g^- value (-60°) toward the *anti* orientation (+180° or -180° respectively). Such values that fell within the range of +90° and +150° (i.e. +120° ± 30°) were labeled as *syn*$^+$ (s^+), indicating that the oxygen of —OH in the carboxyl moiety was in an *syn* orientation arrangement with the proton attached to the β-carbon, positioned at about +120°. Similarly, values that fell within the range of -90° and -150° (i.e. -120° ± 30°) were labeled as *syn*$^-$ (*s*$^-$), indicating that the —OH oxygen of the carboxyl moiety was in *syn* orientation with the proton attached to the β-carbon, positioned at about -120°. It is interesting to note that a $g^- g^+$ sidechain conformer, shown in **Figure 18**, was found in the ε_L backbone conformation, a backbone that is not known to harbour stable conformers.

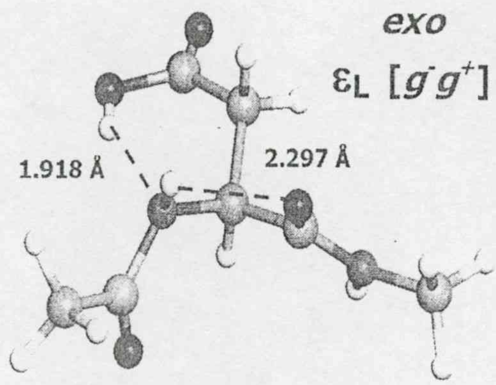

Figure 18 A graphical representation of the stable conformer found at $g^- g^+$ of the ε_L backbone of the *exo* form of the aspartic acid residue.

In this particular $g^- g^+$ conformer, it is found that a backbone-backbone internal hydrogen bond, calculated to be 2.297 Å, may be the stabilizing force needed by the conformer to remain stable. In addition, a rather unusual hydrogen bond, $H^{19}\cdots\cdots N^2$, which has an intermolecular distance of 1.918 Å (result not tabulated but shown in **Figure 18**, may also contribute to the stabilizing force that allows for the existence of this ε_L [$g^- g^+$] conformer. **Figure 19** illustrates the various traditional hydrogen bonds that may exist in the *exo* form of **N**-acetyl-*L*-aspartic acid **N'**-methylamide.

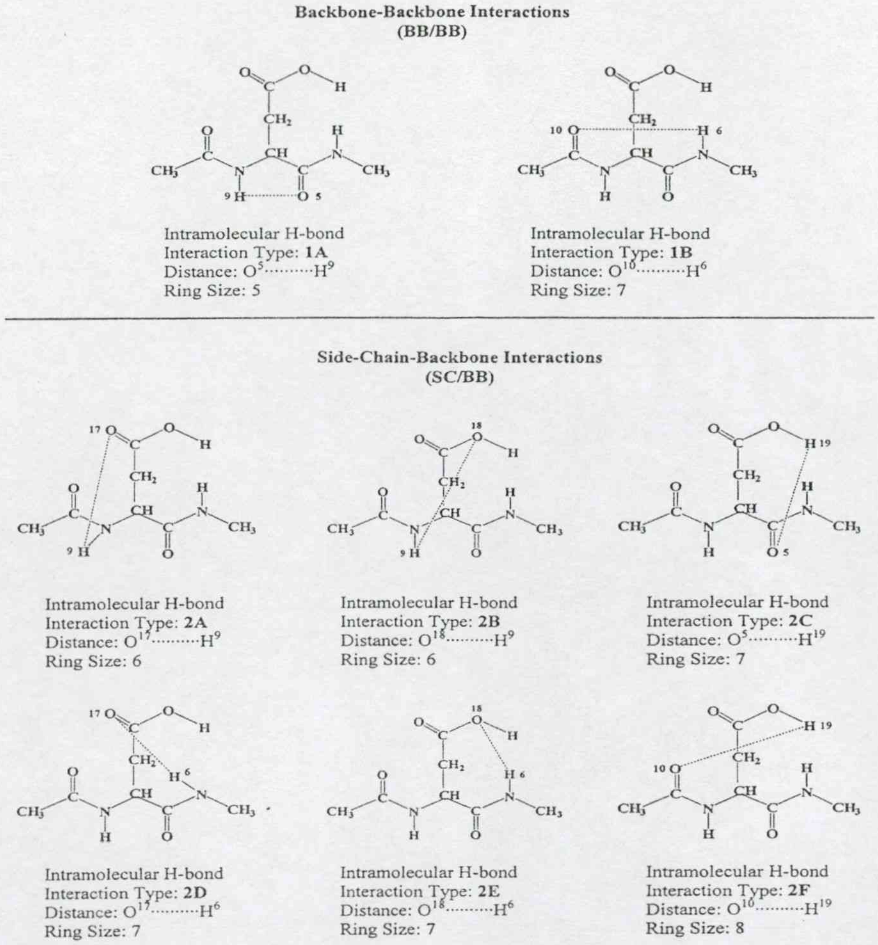

Figure 19 Classification of the types of internal hydrogen bonding for the *exo* form of **N**-acetyl-*L*-aspartic acid **N'**-methylamide.

In this case, since the carboxyl group in the sidechain is in the *exo* form, there is no sidechain-sidechain interaction in the aspartic acid residue. Still, there exist two kinds of stabilizing hydrogen bonds: backbone-backbone (BB/BB) or sidechain-backbone (SC/BB). In total, there are two BB/BB hydrogen bond interactions and six SC/BB hydrogen bond interactions. The corresponding distances for these hydrogen bond interactions are tabulated on **Table 5**.

Table 5

The relative distances of potential hydrogen bonds of **N**-acetyl-*L*-aspartic acid **N'**-methylamide in its *exo* form for all its stable backbone (γ_L, β_L, δ_L, ε_L, γ_D, δ_D, α_D, and ε_D) conformations computed at the B3LYP/6-31G(d) level of theory. No conformers were found for the α_L backbone and hence no hydrogen bond distances for the α_L backbone could be tabulated.

Final Conform.	Interaction Type		Distance (Å) *							
BB [$\chi_1 \chi_2$]	BB/BB	SC/BB	H9-O5	H9-O17	H9-O18	H19-O5	H6-O10	H6-O17	H6-018	H19-O10
γ_L Backbone Conformation										
γ_L [$g^+ g^+$]	1B	2C	3.906	2.344	3.376	1.749	1.917	5.528	5.068	5.421
γ_L [$g^+ g^+$]	1B	2C	3.899	2.342	3.371	1.748	1.916	5.515	5.065	5.430
γ_L [$a\ g^-$]	1B	2C	3.776	4.780	4.809	1.746	1.940	5.610	4.866	5.454
γ_L [$g^- s^-$]	1B	2A	3.880	2.044	3.796	4.863	1.929	5.381	5.973	5.902
β_L Backbone Conformation										
β_L [$g^+ g^+$] [a,b]	1A	-	2.175	3.850	3.943	3.124	5.015	4.888	3.465	5.396
β_L [$g^+ s^-$]	1A	2D, 2F	2.156	4.717	4.271	5.117	5.000	1.977	3.699	1.717
β_L [$a\ a$]	1A	2D	2.046	4.983	5.598	5.767	5.090	1.937	3.847	4.422
β_L [$s^- g^+$]	1A	2F	2.133	5.371	4.819	5.168	5.023	2.434	3.829	1.827
δ_L Backbone Conformation										
δ_L [$s^- g^+$] [a,b]	-	2F	3.532	5.467	4.663	4.779	4.121	5.934	5.150	1.773
δ_L [$g^-\ s$]	-	2F	3.844	4.562	4.047	4.677	3.770	6.205	5.302	1.841
ε_L Backbone Conformation										
ε_L [$g^- g^+$]	1A	-	2.297	4.853	3.402	4.295	4.115	5.002	5.195	3.253
γ_D Backbone Conformation										
γ_D [$g^+ g^+$]	1B	-	4.044	4.364	4.806	3.506	1.810	4.106	2.731	3.086
γ_D [$s^+ g^-$]	1B	2F	3.776	5.537	4.829	4.588	2.225	3.746	2.565	1.713
γ_D [$a\ a$]	1B	-	3.677	4.549	5.637	5.103	1.975	4.773	4.615	4.654
γ_D [$a\ g^-$]	1B	-	3.678	5.186	5.266	3.181	1.934	4.846	3.378	3.970
γ_D [$s^- g^-$]	1B	2C	4.214	4.995	4.763	1.716	1.896	5.732	4.943	5.059
γ_D [$g^-\ a$]	1B	-	4.140	2.740	4.465	5.415	1.876	5.060	5.391	4.661
δ_D Backbone Conformation										
δ_D [$g^+\ a$] [a,b]	-	2D	3.620	3.076	4.641	5.666	4.848	1.942	3.960	4.337
δ_D [$g^+ g^-$] [a,b]	-	2E	3.497	4.848	3.182	4.451	4.853	3.305	2.248	3.376
δ_D [$s^- g^+$]	-	2F	3.450	5.599	4.753	4.740	4.693	5.019	5.204	1.745
δ_D [$g^-\ s$] [a,b]	-	2F	3.425	5.149	4.371	4.654	5.131	4.703	5.027	1.717
α_D Backbone Conformation										
α_D [$g^+ g^+$]	-	2C	4.422	3.685	4.547	1.812	3.005	5.525	4.956	3.173
α_D [$g^+ g^-$]	-	-	4.430	4.908	3.525	4.794	2.764	5.396	5.086	3.222
α_D [$s^- g^-$]	-	2C	4.438	4.677	4.988	1.711	3.000	6.042	5.158	4.608
α_D [$g^-\ a$]	-	-	4.435	2.514	4.288	4.733	3.024	5.034	6.237	4.866
ε_D Backbone Conformation										
ε_D [$a\ a$]	-	2D	2.792	4.800	5.647	5.834	4.824	1.986	3.740	4.491
ε_D [$g^- g^+$]	-	2F	2.727	4.660	4.241	4.776	5.273	4.242	5.246	1.760

[a] After 200 iterations under (TIGHT) at B3LYP/6-31G(d), the force has converged, but the displacement did not converge completely.

[b] This result was obtained from a regular optimization fully converged at B3LYP/6-31G(d).

* Atomic numbering is given in **Figure 2** (right).

It is also interesting to note that in almost all stable conformers, with the exception of $g^+ g^-$ and $g^- a$ in the α_D conformation, there exist at least one type of hydrogen bond interaction. This may suggest that hydrogen bonding, at least in part, contribute significantly to the stability of a conformer for the aspartic acid residue. Here, the BB/BB interaction can be considered as an internal stabilizing factor that allows fundamental stability for the aspartic acid residue while at the same time allowing the sidechain to participate in external interactions with other substrates. On the other hand, the SC/BB interaction can induce even greater internal stability to the aspartic acid residue. An example to illustrate this phenomenon exists in the γ_L [$a\ g^-$] conformation where type 1B (BB/BB) and type 2C (SC/BB) of the hydrogen bond interactions seem to contribute major stabilizing forces that allow for the existence of the conformer at this particular backbone. A correlating trend between hydrogen bond distance and ring size (RS) is shown in **Figure 20**.

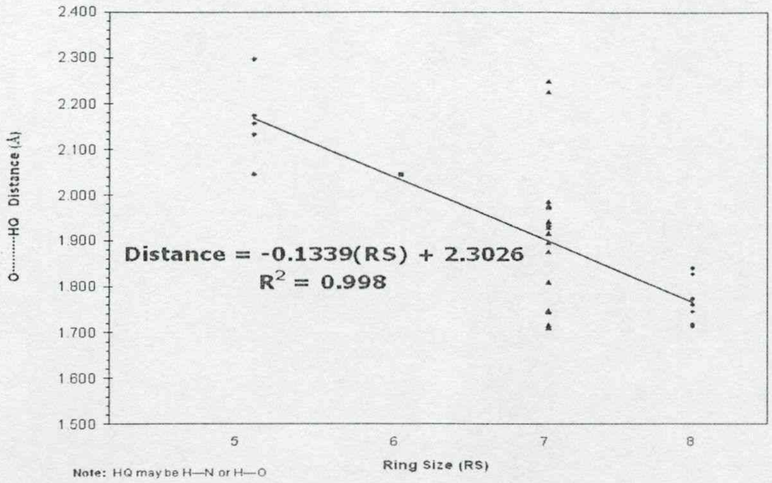

Figure 20 A trend showing the interrelation between hydrogen-bonded distance and ring size (RS) of internal hydrogen bonds for the *exo* form of **N**-acetyl-*L*-aspartic acid **N**'-methylamide. **Note:** HQ may be H—N or H—O.

Here, it is apparent that the shorter the hydrogen bond distance, the greater the RS. The overall correlation equation shows a least square value of $R^2 = 0.998$, showing convincingly that such trend is significant. No Type 2B hydrogen interactions were observed for the aspartic acid residue.

It was also observed that in some cases, the ω_0 torsional angle of the stable conformers (such as those found in the α_D conformation) deviated from the ideal value of 180°. One possible reason for such apparent discrepancy is that there exist strong hydrogen bond interactions that act as stabilizing forces in these conformers. For example, in the α_D [$g^+ g^+$] conformation as well as in *a a* and $g^- g^+$ of the ε_D conformation, where the ω_0 torsional angle deviates the most from the ideal, there exist strong SC/BB interactions (i.e. having hydrogen bond lengths of less than 2.000 Å). This may suggest that as the conformer seeks a stabilizing force, it is willing to rotate its terminal methyl groups, changing its ω_0 torsional angles, in order to form a hydrogen bond interaction that is strong enough to stabilize itself. Also, such observation from the optimization results for **N**-acetyl-*L*-aspartic acid **N**'-methylamide may provide insights on the aspartyl residue's role in the intramolecular interactions of RGD. Such an example may be found in the conformers of the δ_L, δ_D, α_D and ε_D conformations, which possess the SC/BB interactions shown in **Table 5**.

Meanwhile, it is reasonable to infer that an ideal stabilizing situation for the aspartyl residue in a peptide chain would involve both BB/BB as well as SC/BB interactions. In γ_L, β_L, and γ_D conformations, such instances of having both BB/BB and SC/BB interactions exist. Interestingly, these three backbones are traditionally recognized as where most of the stable conformers for an amino acid would be located in computations not involving solvation. The study of SC/BB and BB/BB interactions in N-acetyl-*L*-aspartic acid N'-methylamide may deem significant as these interactions may represent the internal stabilizing force within a peptide chain when it is bound to a substrate, such as a receptor (charged or uncharged). The fact that 19 out of the 27 optimized conformers for the *exo* form of N-acetyl-*L*-aspartic acid N'-methylamide possess a SC/BB interaction suggests that the ability of the aspartic acid residue to form an external hydrogen bond, whether to itself, to an adjacent neighbour, or to a binding substrate, may be significant to the molecule's stability as well as the relative stability of a binding assay involving the amino acid. External hydrogen bondings are significant when the aspartyl residue participates in intra- or inter-molecular interactions, such as in the RGD tripeptide. This way, the presence or absence of these stabilizing forces may directly affect the folding patterns of the RGD tripeptide moiety. Here, while the BB/BB interaction may be considered as an internal stabilizing factor for the *exo* form of the aspartic acid residue, its sidechain can participate in external interactions with other substrates. This phenomenon can be applied to the docking of a specific molecule to receptors that express the aspartic acid residue on its surface. This way, one can explain why a point mutation in a receptor will significantly affect its recognition capabilities for certain ligands. This proposed mechanism does not imply that the *endo* form of the aspartic acid residue are "useless" in such receptor/ligand binding. Rather, it suggests that while the sidechain of the aspartic acid residue is stabilized by its SC/SC hydrogen bond, it is still possible for its backbone to participate in either external or internal stabilizing interactions. These suggestions point to the fact that *ab initio* studies for single amino acid residues may be useful in experiments involving protein bindings, receptor/ligand recognition, as well as *de novo* drug designs in a biological system.

5.1.2.2 Energetics of the Exo Form of Aspartic Acid

Figure 12 of reference 52, various stabilization energies, with respect to either β_L or γ_L of the glycine residue, are shown in a bar-graph format. The difference in stabilization energy, ΔE^{stabil}, with respect to β_L and with respect to γ_L is constant (1.13 kcal/mol), as shown in **Figure 10**. Again, the values with respect to the β_L glycine residue will be discussed.

One can observe that the L subscripted conformations (i.e. β_L, δ_L, ε_L, γ_L) of the aspartic acid residue are stabilized more extensively than its D subscripted forms (i.e. α_D,γ_D, δ_D, ε_D). As illustrated in Figure 12[52], most of the stabilization energies for the L conformers, having a more negative value, indicated that the conformers are truly stabilized. This is shown by the fact that the L subscripted conformers for N-acetyl-*L*-aspartic acid N'-methylamide either have great negative values or small positive values for their stabilization energies. This trend is observed in the γ_L, β_L δ_L and ε_L backbones for the aspartic acid residue. On the other hand, most conformers found for the D subscripted form of the aspartic acid residue are de-stabilized. Again, the D-subscripted conformers, shown in Figure 12[52], have either great positive values or small negative values for their stabilization energies. This trend exists in the α_D, γ_D, δ_D and ε_D backbones for the aspartic acid residue. Even though the ε_L and the ε_D conformers seem to represent an apparent exception to the trend (where both L and D subscripted conformers appeared to be stabilized), nevertheless, the actual magnitudes for their ΔE^{stabil} still followed the trend outlined above.

5.2 Aspartate Ion

5.2.1 Molecular Geometry of the Aspartate Ion

Shown in **Table 6** are all optimized results, which include the dihedral angles, the relative energies as well as the stabilization energies, for all stable conformers found for N-acetyl-*L*-aspartate-N'-methylamide. Of the possible 81 initial structures expected to be found for N-acetyl-*L*-aspartate-N'-methylamide, only 7 stable conformers were found at the B3LYP/6-31G(d) level. These stable conformers were found in only four of the nine possible backbone conformations: γ_L, β_L, α_L, α_D.

Table 6

Geometric and energetic parameters of optimized conformers of **N**-acetyl-*L*-aspartate-**N'**-methylamide for all its stable backbone (γ_L, β_L, α_L, and α_D) conformations computed at the B3LYP/6-31G(d) level of theory. Shown here are the optimized torsional angles, computed energy values, relative energies, and stabilization energies.

Final Conform.	Optimized Parameters												
BB [χ_1 χ_2]	ϕ	ψ	ω_0	ω_1	χ_1	χ_2	r[C-O]	χ_2*	R[C-O*]	E_{min} (hartree)	ΔE (kcal/mol)	ΔE^{stabil} (kcal) γL	ΔE^{stabil} (kcal) βL
γ_L [g^+ s]	-81.09	59.08	-173.78	-177.88	36.39	-24.55	1.281	159.30	1.239	-683.8711687	5.441	-23.127	-24.259
γ_L [g^- g^+]	-80.85	69.00	-165.80	-173.75	-39.99	48.94	1.283	-134.18	1.240	-683.8732396	4.141	-24.427	-25.558
β_L [a s]	-155.74	174.13	175.95	175.26	-164.36	-12.53	1.279	167.23	1.241	-683.8760086	2.404	-26.164	-27.296
α_L [g^+ s^+]	-108.55	-114.69	-172.61	177.10	55.82	105.39	1.262	-71.10	1.261	-683.8755999	2.660	-25.908	-27.039
α_L [g^+ s]	-102.59	-53.41	-179.41	-173.68	48.08	-1.22	1.286	179.71	1.238	-683.8798393	0.000	-28.568	-29.699
α_L [g^- g^+]	-70.78	-28.54	-167.10	175.83	-46.91	45.15	1.279	-138.03	1.241	-683.8696728	6.254	-22.314	-23.445
α_D [g^- s]	54.89	41.00	154.07	-167.14	-54.75	21.29	1.281	-159.71	1.242	-683.8613062	11.630	-16.938	-18.070

Note that no stable conformers could be found for the δ_L, ε_L, γ_D, δ_D, and ε_D backbone conformations at this level of theory.

The double-scan PEHSs for these backbones reveal numerous minima on the landscape and contour representations, shown in **Figure 21 - Figure 24**.

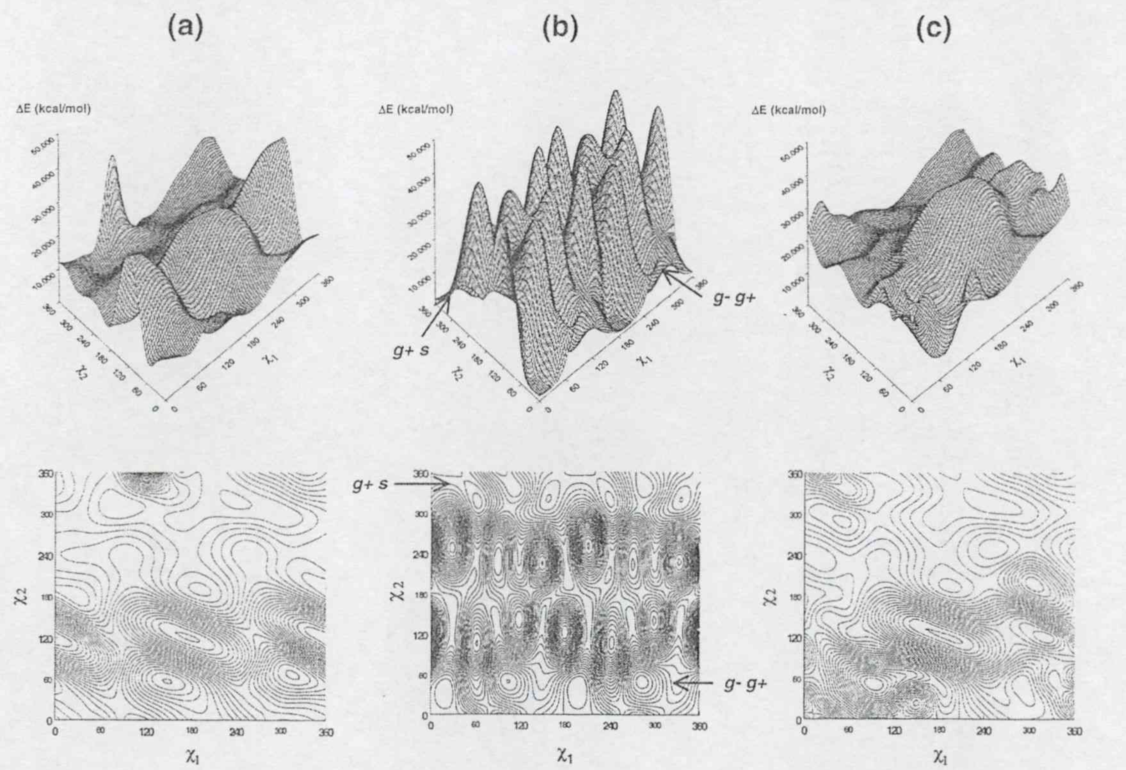

Figure 21 Double-scan PES, E = E (χ_1, χ_2), generated for the γ_L backbone conformation of: (a) the *endo* form of **N**-acetyl-*L*-aspartic acid-**N'**-methylamide, (b) **N**-acetyl-*L*-aspartate-**N'**-methylamide, (c) the *exo* form of **N**-acetyl-*L*-aspartic acid-**N'**-methylamide in both landscape (top) and contour (bottom) representations. Torsional angles χ_1 and χ_2 are given in degrees from 0° to 360°.

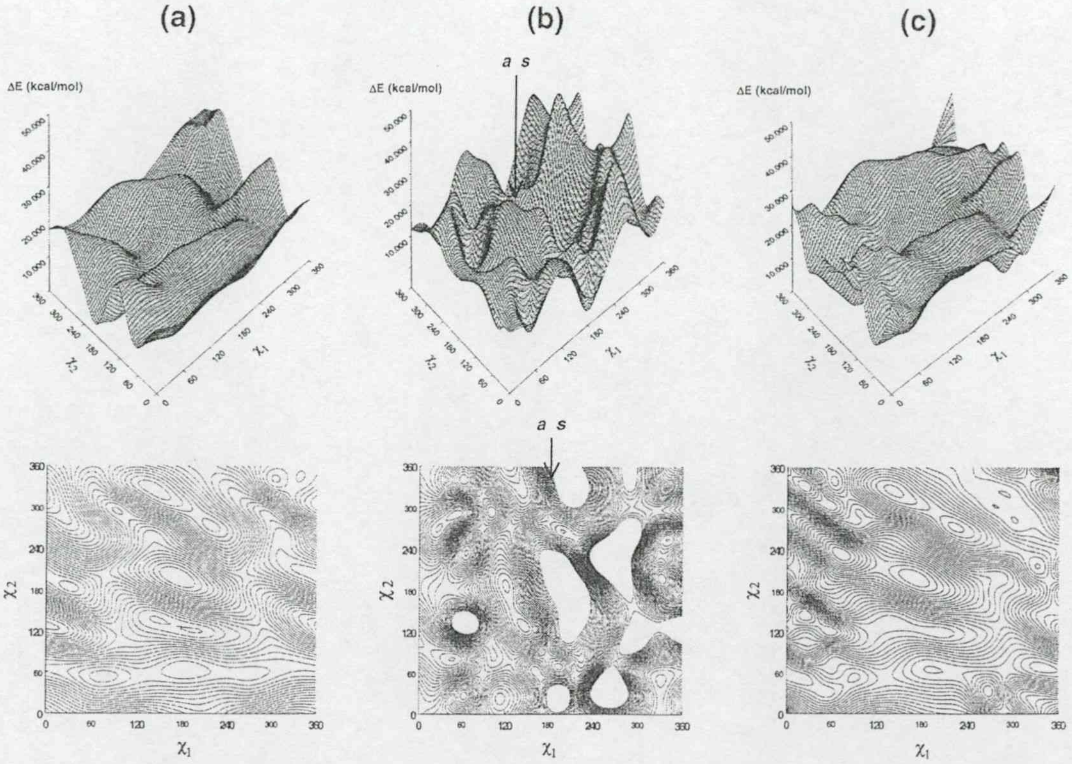

Figure 22 Double-scan PES, E = E (χ_1, χ_2), generated for the β_L backbone conformation of: (a) the *endo* form of **N**-acetyl-*L*-aspartic acid-**N'**-methylamide, (b) **N**-acetyl-*L*-aspartate-**N'**-methylamide, (c) the *exo* form of **N**-acetyl-*L*-aspartic acid-**N'**-methylamide in both landscape (top) and contour (bottom) representations. Torsional angles χ_1 and χ_2 are given in degrees from 0° to 360°.

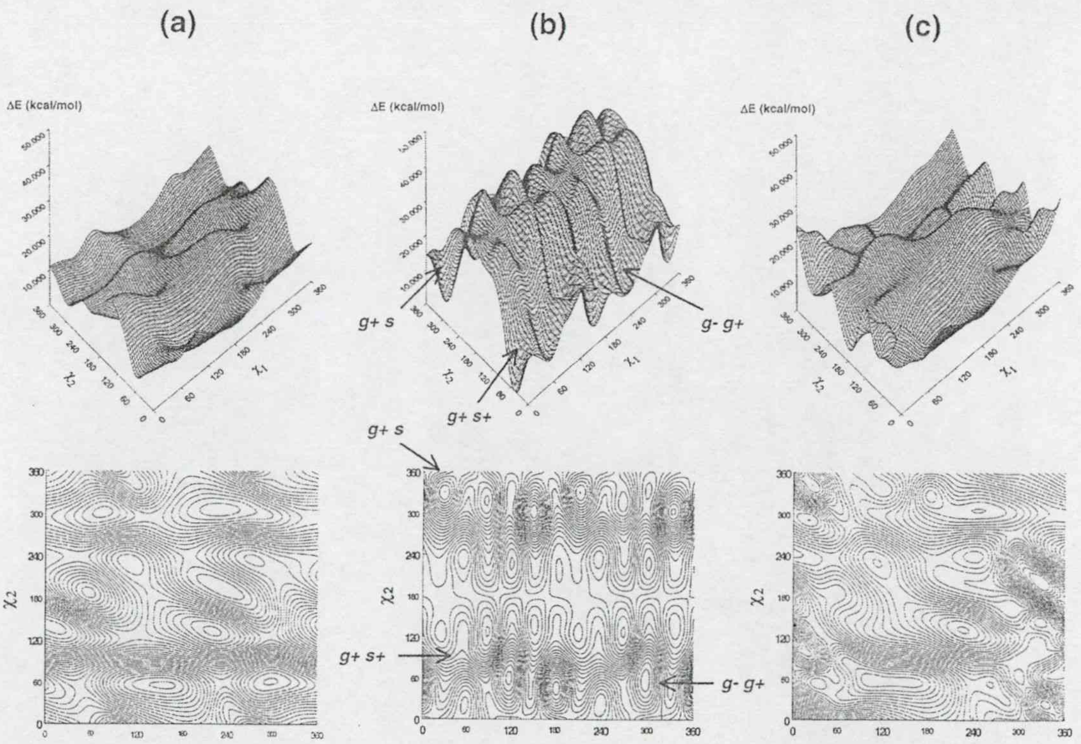

Figure 23 Double-scan PES, E = E (χ_1, χ_2), generated for the α_L backbone conformation of: (a) the *endo* form of **N**-acetyl-*L*-aspartic acid-**N'**-methylamide, (b) **N**-acetyl-*L*-aspartate-**N'**-methylamide, (c) the *exo* form of **N**-acetyl-*L*-aspartic acid-**N'**-methylamide in both landscape (top) and contour (bottom) representations. Torsional angles χ_1 and χ_2 are given in degrees from 0° to 360°.

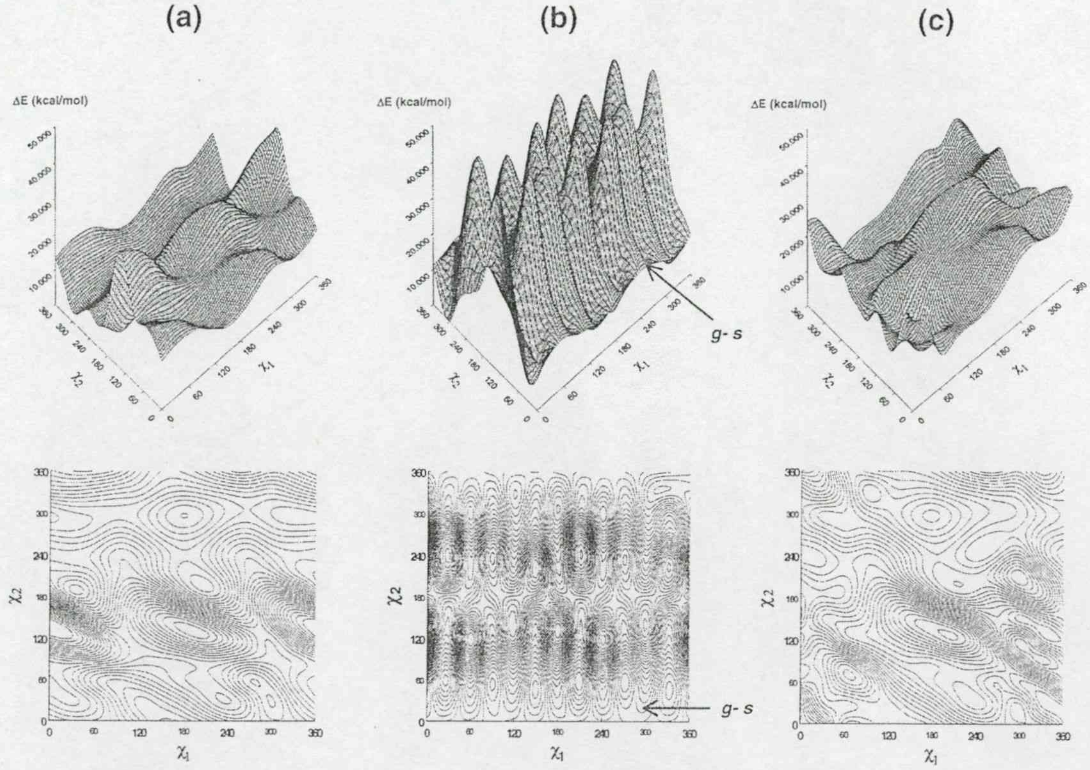

Figure 24 Double-scan PES, E = E (χ_1, χ_2), generated for the α_D backbone conformation of: (a) the *endo* form of N-acetyl-*L*-aspartic acid-N'-methylamide, (b) N-acetyl-*L*-aspartate-N'-methylamide, (c) the *exo* form of N-acetyl-*L*-aspartic acid-N'-methylamide in both landscape (top) and contour (bottom) representations. Torsional angles χ_1 and χ_2 are given in degrees from 0° to 360°.

However, only some of these points can be considered as "true" minima since any minimum found on a particular PES can only be considered as a semi-rigid optimization. Minima that are not confirmed by subsequent *ab initio* optimizations can only be regarded as "false" points on the hypersurface and may represent higher order critical points such as those for transition state structures. There are two reasons why "false" minima occurred on the PEHS for N-acetyl-*L*-aspartate-N'-methylamide: 1) both ϕ and ψ torsional angles were frozen during the double-scan calculations; and 2) both χ_1 and χ_2 were optimized at fixed 30° increments (from 0° to 360°) while the ϕ and ψ torsional angles were fixed. As mentioned earlier, the backbone geometry of N-acetyl-*L*-aspartate-N'-methylamide is expected to be similar to that of the alanyl residue. Since previous *ab initio* studies on the alanine molecule (3-8) have reported that most stable conformers were found in the γ_L, β_L and γ_D backbone conformations, it is somewhat surprising to learn that no conformers were found in the γ_D backbone of the aspartate residue. Unexpectedly, of the 7 stable conformers found for the aspartate residue, 3 were located in the α_L backbone, a conformation that is not known to harbour stable structures in most amino acids. More surprising, however, is the fact that the global minimum for **N**-acetyl-*L*-aspartate-**N'**-methylamide occurred in the α_L backbone conformation (**Figure 25**) and not in the γ_L backbone where global minima were usually located.

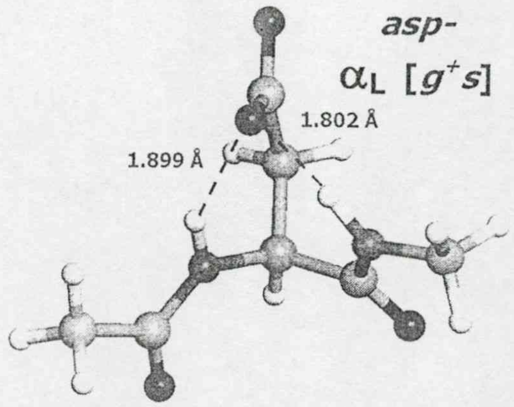

Figure 25 A graphical representation of the global minimum found at the α_L [g^+ s] backbone conformation of the aspartate residue.

These observations can be linked to the findings by Deane *et al.*[61], who reported that the α_L region on the Ramachandran plot is readily adopted by the aspartic acid residue in an experiment involving carbonyl-carbonyl interactions.

For this dissertation, it was initially expected that the proton affinity of **N**-acetyl-*L*-aspartate-**N'**-methylamide could be defined by matching the optimized parameters of stable geometric structures against those optimized in the *endo* and *exo* forms of **N**-acetyl-*L*-aspartic acid-**N'**-methylamide. However, 37 and 27 stable conformers were respectively found for the *endo* and *exo* forms of the aspartic acid residue at the B3LYP/6-31G(d) level of theory, compared to the 7 stable structures found for the aspartate. Clearly, the number of stable conformers found in both *endo* and *exo* forms of **N**-acetyl-*L*-aspartic acid-**N'**-methylamide far exceed those found in **N**-acetyl-*L*-aspartate-**N'**-methylamide, suggesting that the complexity of the protonation pattern for the aspartate residue far exceeds the initial hypothesis.

5.2.2 Molecular Energetics of the Aspartate Ion

Comparing the energies (E_{min}) of the conformers found for the aspartate residue against those found for the aspartic acid residue provides some clues to explaining the dilemma concerning the aspartate protonation pattern (**Table 7 – Table 10**).

Table 7

Deprotonation energies found for the *endo* and *exo* conformers of N-acetyl-*L*-aspartic acid-N'-methylamide against conformers optimized for N-acetyl-*L*-aspartate-N'-methylamide in the γ_L backbone conformation at the B3LYP/6-31G(d) level of theory.

aspartate	E_{min} (hartree)	aspartic acid *endo*	E_{min} (hartree)	vs γ_L $[g^+\ s]$ (hartree)	vs γ_L $[g^+\ s]$ ΔE (kcal/mol)	vs γ_L $[g^-\ g^+]$ (hartree)	vs γ_L $[g^-\ g^+]$ ΔE (kcal/mol)
γ_L $[g^+\ s]$	-683.8711687	γ_L $[g^+ s^+]$	-684.4260542	0.5549	348.1959	0.5528	346.8964
γ_L $[g^- g^+]$	-683.8732396	γ_L $[g^+ g^-]$	-684.4210847	0.5549	348.1959	0.5478	343.7780
		γ_L $[a\ \ s]$	-684.4178720	0.5499	345.0775	0.5446	341.7620
		γ_L $[a\ \ a]$	-684.4199177	0.5487	344.3452	0.5467	343.0457
		γ_L $[g^- s^+]$	-684.4190950	0.5479	343.8290	0.5459	342.5294
		γ_L $[g^-\ a]$	-684.4189046	0.5477	343.7095	0.5457	342.4100
		γ_L $[g^- s^-]$	-684.4217674	0.5506	345.5059	0.5485	344.2064
		aspartic acid *exo*	E_{min} (hartree)	vs γ_L $[g^+\ s]$ (hartree)	vs γ_L $[g^+\ s]$ ΔE (kcal/mol)	vs γ_L $[g^-\ g^+]$ (hartree)	vs γ_L $[g^-\ g^+]$ ΔE (kcal/mol)
		γ_L $[g^+ g^+]$	-684.4265160	0.5553	348.4857	0.5533	347.1862
		γ_L $[g^+ g^+]$	-684.4266579	0.5555	348.5748	0.5534	347.2752
		γ_L $[a\ g^-]$	-684.4208809	0.5497	344.9496	0.5476	343.6501
		γ_L $[g^- s^-]$	-684.4126227	0.5415	339.7675	0.5394	338.4680

Table 8

Deprotonation energies found for the *endo* and *exo* conformers of N-acetyl-*L*-aspartic acid-N'-methylamide against conformers optimized for N-acetyl-*L*-aspartate-N'-methylamide in the β_L backbone conformation at the B3LYP/6-31G(d) level of theory.

aspartate	E_{min} (hartree)	aspartic acid *endo*	E_{min} (hartree)	vs β_L $[a\ \ s]$ (hartree)	vs β_L $[a\ \ s]$ ΔE (kcal/mol)
β_L $[a\ \ s]$	-683.8760086	β_L $[g^+ s^+]$	-684.4154168	0.5394	338.4838
		β_L $[g^+\ \ a]^{a,b}$	-684.4153786	0.5394	338.4598
		β_L $[a\ g^+]$	-684.4184974	0.5425	340.4169
		β_L $[a\ \ a]$	-684.4240236	0.5480	343.8846
		aspartic acid *exo*	E_{min} (hartree)	vs βL [a s] (hartree)	vs β_L $[a\ \ s]$ ΔE (kcal/mol)
		β_L $[g^+ g^+]^{a,b}$	-684.4058456	0.5298	332.4778
		β_L $[g^+ s^-]$	-684.4201077	0.5441	341.4274
		β_L $[a\ \ a]$	-684.4161709	0.5402	338.9570
		β_L $[s^- g^+]$	-684.4237651	0.5478	343.7224

Table 9

Deprotonation energies found for the *endo* and *exo* conformers of N-acetyl-*L*-aspartic acid-N'-methylamide against conformers optimized for N-acetyl-*L*-aspartate-N'-methylamide in the α_L backbone conformation at the B3LYP/6-31G(d) level of theory.

aspartate	E_{min} (hartree)	aspartic acid *endo*	E_{min} (hartree)	vs α_L $[g^+s^+]$ (hartree)	vs α_L $[g^+s^+]$ ΔE (kcal/mol)	vs α_L $[g^+\ s]$ (hartree)	vs α_L $[g^+\ s]$ ΔE (kcal/mol)
α_L $[g^+ s^+]$	-683.8755999	α_L $[g^- s^-]^{a,b}$	-684.4153827	0.5398	338.7188	0.5355	336.0586
α_L $[g^+\ s]$	-683.8798393	aspartic acid *exo*	E_{min} (hartree)	vs α_L $[g^+s^+]$ (hartree)	vs α_L $[g^+s^+]$ ΔE (kcal/mol)	vs α_L $[g^+\ s]$ (hartree)	vs α_L $[g^+\ s]$ ΔE (kcal/mol)
α_L $[g^- g^+]$	-683.8698728						

[a] After 200 iterations under (TIGHT) at B3LYP/6-31G(d), the force has converged, but the displacement did not converge completely.

[b] This result was obtained from a regular optimization fully converged at B3LYP/6-31G(d).

Table 10

Deprotonation energies found for the *endo* and *exo* conformers of **N**-acetyl-*L*-aspartic acid-**N'**-methylamide against conformers optimized for **N**-acetyl-*L*-aspartate-**N'**-methylamide in the α_D backbone conformation at the B3LYP/6-31G(d) level of theory.

aspartate	E_{min} (hartree)	aspartic acid *endo*	E_{min} (hartree)	vs α_D [$g^- s$] (hartree)	vs α_D [$g^- s$] ΔE (kcal/mol)
α_D [$g^- s$]	-683.8613062	α_D [$g^+ s^+$]	-684.4070563	0.5458	342.4634
		α_D [$g^+ g^-$]	-684.4040903	0.5428	340.6022
		α_D [$a\ g^+$]	-684.4097827	0.5485	344.1742
		α_D [$a\ s^-$]	-684.4122840	0.5510	345.7438
		α_D [$g^-\ s$]	-684.4119363	0.5506	345.5256
		α_D [$g^-\ a$]	-684.4166005	0.5553	348.4524
		aspartic acid *exo*	E_{min} (hartree)	vs α_D [$g^- s$] (hartree)	vs α_D [$g^- s$] ΔE (kcal/mol)
		α_D [$g^+ g^+$]	-684.4118612	0.5506	345.4785
		α_D [$g^+ g^-$]	-684.3904410	0.5291	332.0371
		α_D [$s^- g^-$]	-684.4145135	0.5532	347.1428
		α_D [$g^-\ a$]	-684.4094323	0.5481	343.9543

From **Table 7 – Table 10**, it is clear that the energy difference between aspartate conformers and aspartic acid conformers is approximately 340 kcal/mol (or 0.54 hartree). This means that protonating the aspartate residue may stabilize the overall geometry of each conformer optimized, since the protonated aspartic acid has lower energies than the deprotonated aspartate. More noticeably, however, is the difference between the stabilization energy exerted by the sidechain on the backbone for the aspartate and aspartic acid residues (**Table 6, Table 2 and Table 4**). When comparing the stabilization energy values between **Table 6, Table 2 and Table 4**, it is clear that the aspartate sidechain, while losing its proton, can stabilize its backbone geometry in a greater extent than the aspartic acid sidechain. If this is the case, then it suggests that when deprotonated, the lone electron in the negatively charged aspartate sidechain allows for greater stabilization effects on its backbone than the aspartic acid sidechain. In this scenario, both r[C—O] and R[C—O*] may participate in hydrogen bond interactions with the backbone atoms and stabilizing the backbone geometry.

5.3 Intrinsic Sidechain Acidity of Aspartic Acid Residue

When protonating the aspartate residue, there are more geometric choices by which the proton can dock itself (**Figure 26**).

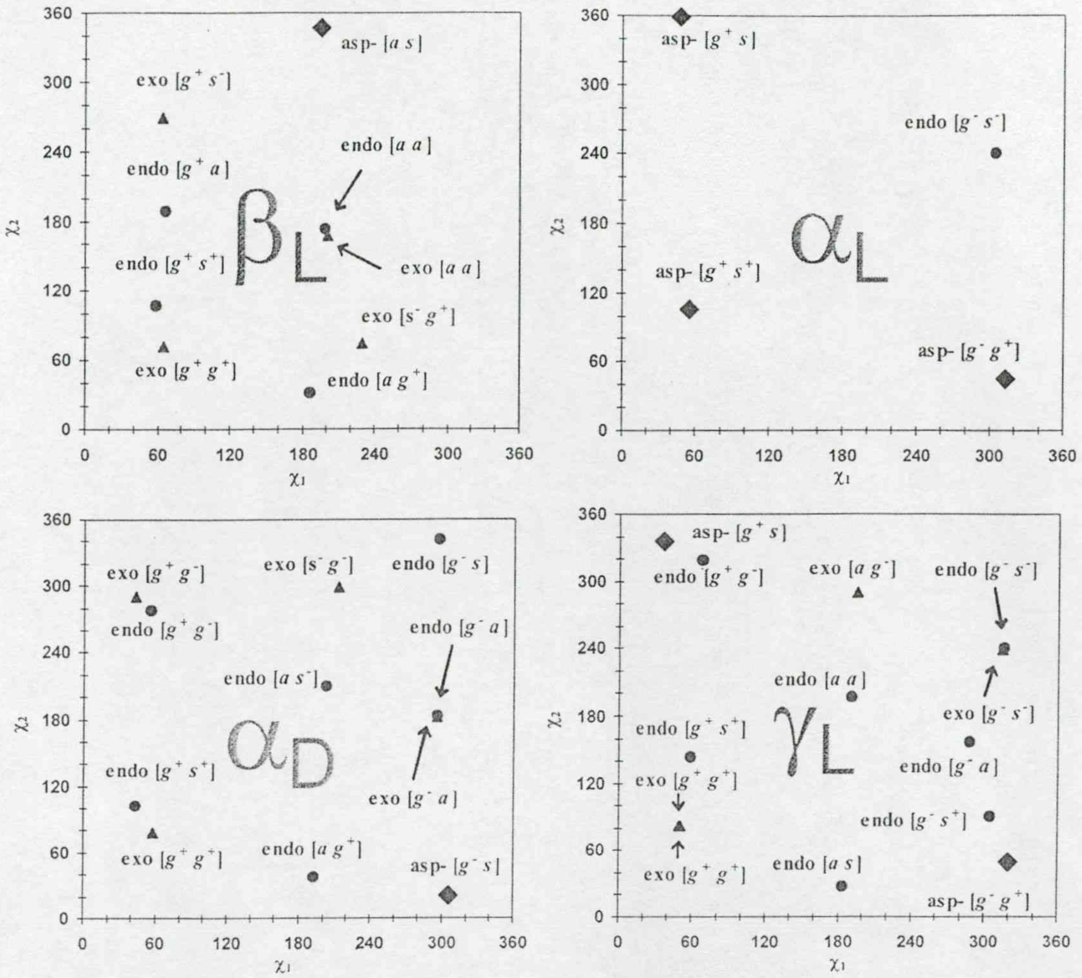

Figure 26 Scatter-plot diagrams showing the optimized conformers found for **N**-acetyl-*L*-aspartate-**N'**-methylamide and the *endo* and *exo* forms of **N**-acetyl-*L*-aspartic acid-**N'**-methylamide in the γ_L, α_L, α_D, and β_L backbone conformations. Note: rhombus represents **N**-acetyl-*L*-aspartate-**N'**-methylamide, circle represents the *endo* form of **N**-acetyl-*L*-aspartic acid-**N'**-methylamide, and triangles represent the *exo* form of **N**-acetyl-*L*-aspartic acid-**N'**-methylamide

As shown in **Figure 26**, there are, in general, more *endo* and *exo* conformers of the aspartic acid residue surrounding the aspartate conformers in most backbone conformations. Interestingly, however, there are 3 aspartate conformers found for the α_L backbone conformation while only one stable conformer was found in both *endo* and *exo* forms of the aspartic acid (**Figure 26**). This finding may suggest that a particular aspartic acid conformer might need to change its backbone conformation before it can be deprotonated into a stable aspartate form.

Figure 27 shows the traditional hydrogen interactions that may exist in **N**-acetyl-*L*-aspartate-**N'**-methylamide.

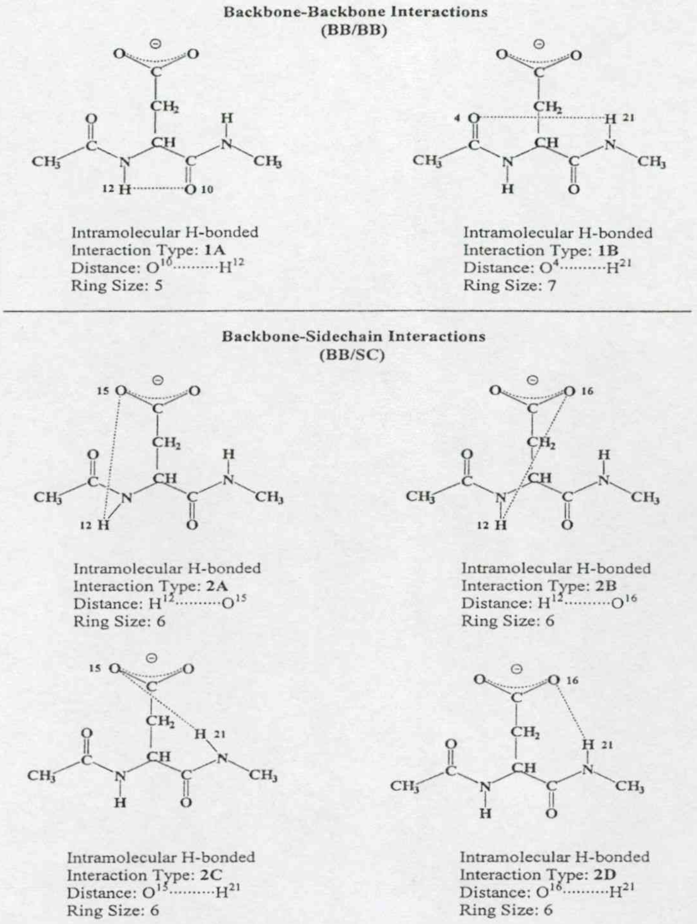

Figure 27 Classification of the "traditional" hydrogen bond interactions for **N**-acetyl-*L*-aspartate-**N'**-methylamide.

The various types of hydrogen bond interactions were tabulated in **Table 11**. There were two backbone-backbone (BB/BB) and four backbone-sidechain (BB/SC) interactions. Although hydrogen bonding represents only weak interactions in inter- and intra- molecular structures, their presence is still significant and especially in ligand binding and protein-ligand recognitions. If the aspartyl residue was coded in a receptor or an ion channel, BB/BB interactions may help stabilize the aspartyl residue in a peptide chain, BB/SC interactions would allow for ligand binding and recognition by forming an overall stable structure with the ligand. In addition, since the aspartyl residue is involved in the RGD tripeptide, these hydrogen bond interactions may be significant in peptide folding, where both BB/BB and BB/SC interactions might be important in forming stabilized structures. Here, the aspartate sidechain may stabilize the RGD backbone to an even greater extent than does its protonated form.

Table 11

The relative distances of potential hydrogen bonds of **N**-acetyl-*L*-aspartate-**N**'-methylamide for all its stable backbone (γ_L, β_L, α_L, and α_D) conformations computed at the B3LYP/6-31G(d) level of theory. No conformers were found for the δ_L, ε_L, γ_D, δ_D, and ε_D backbone conformations and hence no hydrogen bond distances for these backbones could be tabulated.

Final Conform.	Interaction Type		Distance (Å) *					
BB [χ_1 χ_2]	BB/BB	SC/BB	H12-O10	H12-O15	H12-O16	H21-O4	H21-O15	H21-016
γ_L [g^+ s]	1B	2A	3.782	1.561	3.484	1.896	4.894	6.074
γ_L [g^-g^+]	1B	2A	3.982	1.583	3.441	1.844	5.171	6.060
β_L [a s]	1A	2C	2.021	4.926	5.530	5.129	1.601	3.524
α_L [g^+s^+]	-	2B, 2C	3.734	3.489	1.912	5.439	1.832	3.278
α_L [g^+ s]	-	2A, 2C	4.066	1.899	3.643	4.764	1.802	3.552
α_L [g^-g^+]	-	2A	4.417	1.632	3.518	3.082	4.331	5.558
α_D [g^- s]	-	2A	4.368	1.693	3.633	2.721	4.810	6.142

* Atomic numbering is given in **Figure 6**.

As shown in **Table 11**, all stable conformers of the aspartate residue have at least one type of hydrogen bond interaction. Because it is an anion, the aspartate sidechain may participate in more hydrogen bond interactions than the aspartic acid sidechain; and each atom in the aspartate molecule will repel against one another to a greater extent than in the aspartic acid residue. Clearly, this situation will cause the overall bond length to be somewhat longer in aspartate than in aspartic acid, resulting in higher energies for the aspartate conformers.

By subtracting the PEHSs of the *endo* and *exo* forms of **N**-acetyl-*L*-aspartic acid-**N'**-methylamide from that of **N**-acetyl-*L*-aspartate-**N'**-methylamide in their respective backbone conformations (γ_L, β_L, α_L, α_D), the "vertical" deprotonation PEHS of N-acetyl-*L*-aspartic acid-N'-methylamide can be found (**Figure 28 – Figure 31**). In general, the deprotonation patterns of both *endo* and *exo* forms of N-acetyl-*L*-aspartic acid-**N'**-methylamide were similar, where the PEHSs show similar minima and maxima. The greatest difference in deprotonation patterns for both the *endo* and *exo* forms of the aspartic acid residue was shown in the β_L backbone conformation (**Figure 29 (a) and (c)**).

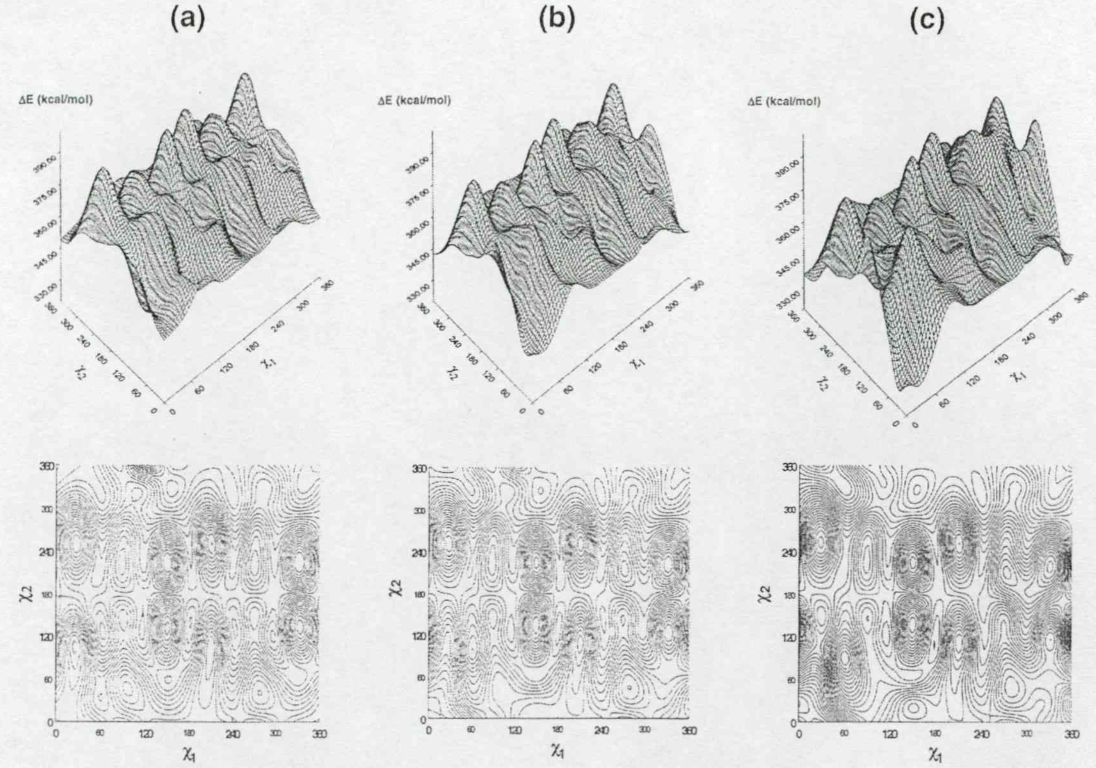

Figure 28 Double-scan PES, E = E (χ_1, χ_2), generated for the deprotonation energie of (a) the *endo*, (b) the average deprotonation energies of both the *endo* and the *exo* forms, and (c) the *exo* forms of **N**-acetyl-*L*-aspartic acid-**N'**-methylamide in its γ_L backbone conformation. Torsional angles χ_1 and χ_2 are given in degrees from 0° to 360°.

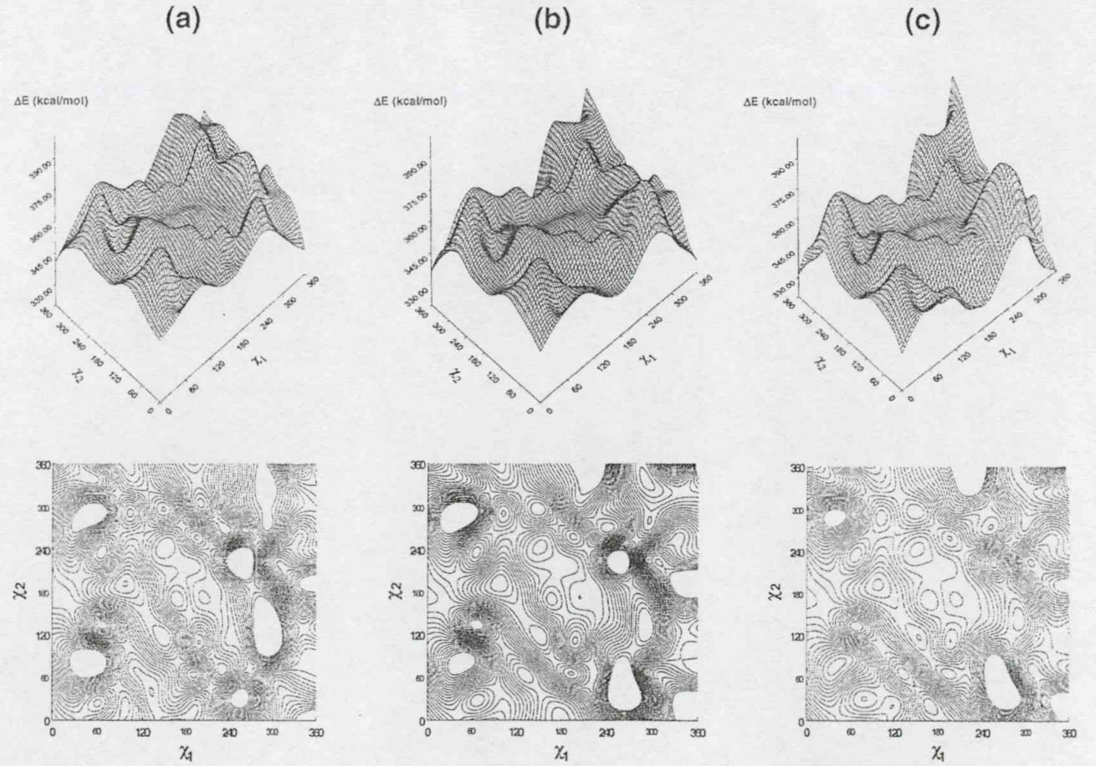

Figure 29 Double-scan PES, E = E (χ_1, χ_2), generated for the deprotonation energie of (a) the *endo*, (b) the average deprotonation energies of both the *endo* and the *exo* forms, and (c) the *exo* forms of **N**-acetyl-*L*-aspartic acid-**N'**-methylamide in its β_L backbone conformation. Torsional angles χ_1 and χ_2 are given in degrees from 0° to 360°.

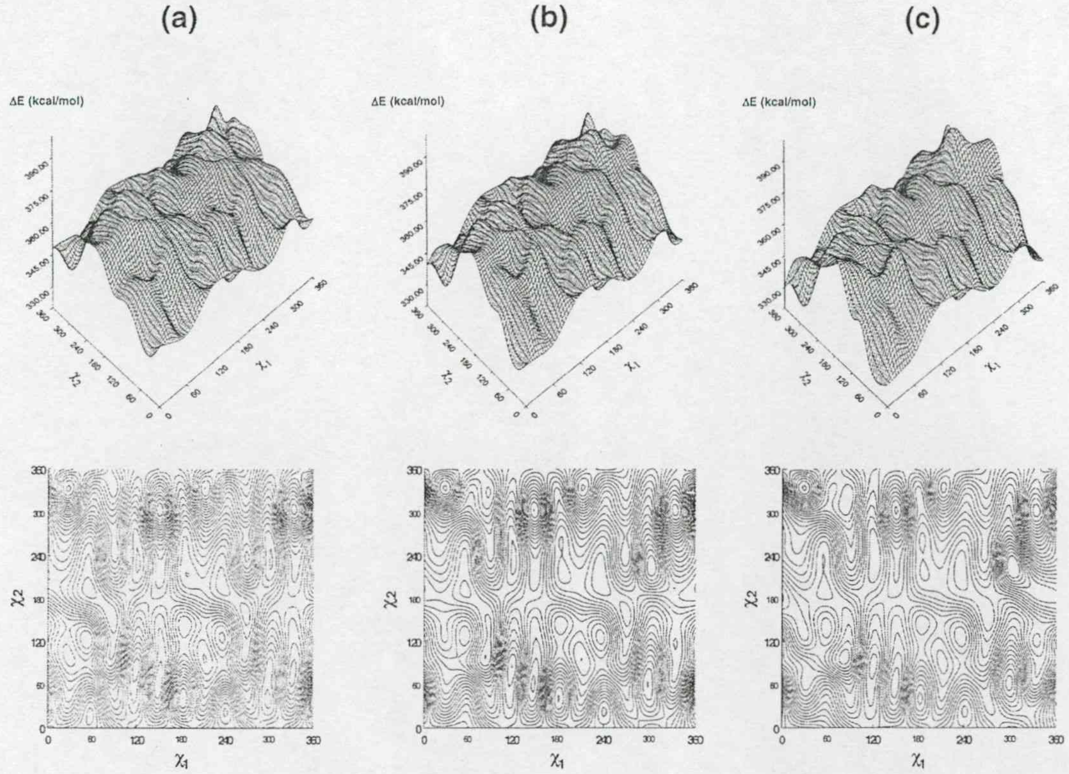

Figure 30 Double-scan PES, E = E (χ_1, χ_2), generated for the deprotonation energie of (a) the *endo*, (b) the average deprotonation energies of both the *endo* and the *exo* forms, and (c) the *exo* forms of **N**-acetyl-*L*-aspartic acid-**N'**-methylamide in its α_L backbone conformation. Torsional angles χ_1 and χ_2 are given in degrees from 0° to 360°.

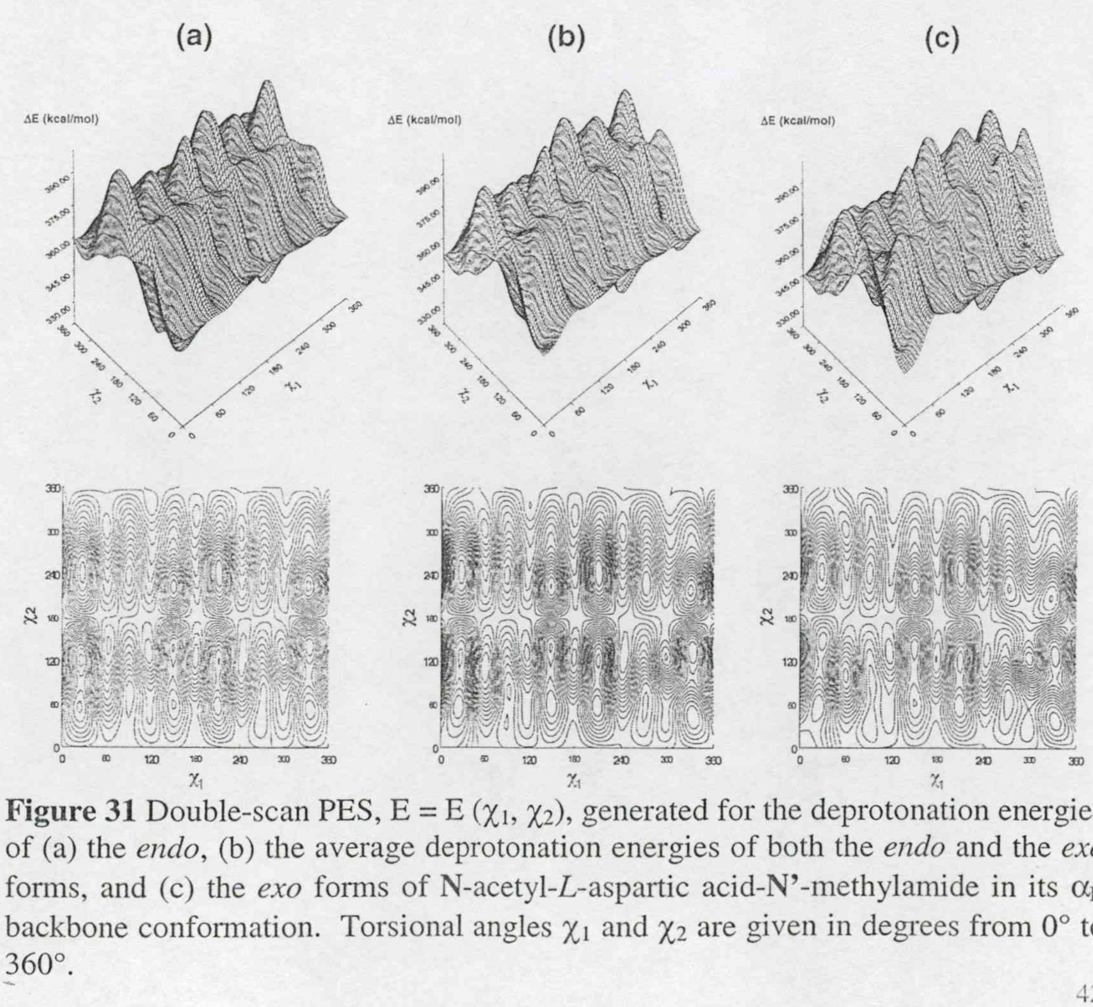

Figure 31 Double-scan PES, E = E (χ_1, χ_2), generated for the deprotonation energies of (a) the *endo*, (b) the average deprotonation energies of both the *endo* and the *exo* forms, and (c) the *exo* forms of **N**-acetyl-*L*-aspartic acid-**N'**-methylamide in its α_D backbone conformation. Torsional angles χ_1 and χ_2 are given in degrees from 0° to 360°.

In closing, it should be emphasized that aspartate sidechain surfaces were possible to compute for the γ_L, β_L, α_L and α_D backbone conformations. However, such surfaces could not be generated for the remaining five backbone conformations. All attempts failed because many of the points were considerably higher (data not shown) than the normal deprotonation energy. For this reason it seems that the aspartic acid residue would rather change conformation to the favourable backbone structures (γ_L, β_L, α_L, α_D) before it would undergo deprotonation. In this case, a conformer of the aspartic acid residue in the δ_L, ε_L, γ_D, δ_D, and ε_D backbone conformations (where no stable conformers could be found for the aspartate residue) would migrate to one of its nearest neighbours (γ_L, β_L, α_L, or α_D) by changing either the ϕ or the ψ torsional angles. These "nearest neighbours" also represent the "allowed" backbone conformations where stable conformers of aspartate residue were found (γ_L, β_L, α_L, and α_D). This model is illustrated in **Figure 32**, where there are three backbone conformations (γ_D, δ_D, and ε_D) with two nearest "allowed" neighbours and two backbone conformations (δ_L and ε_L) with three nearest "allowed" neighbours.

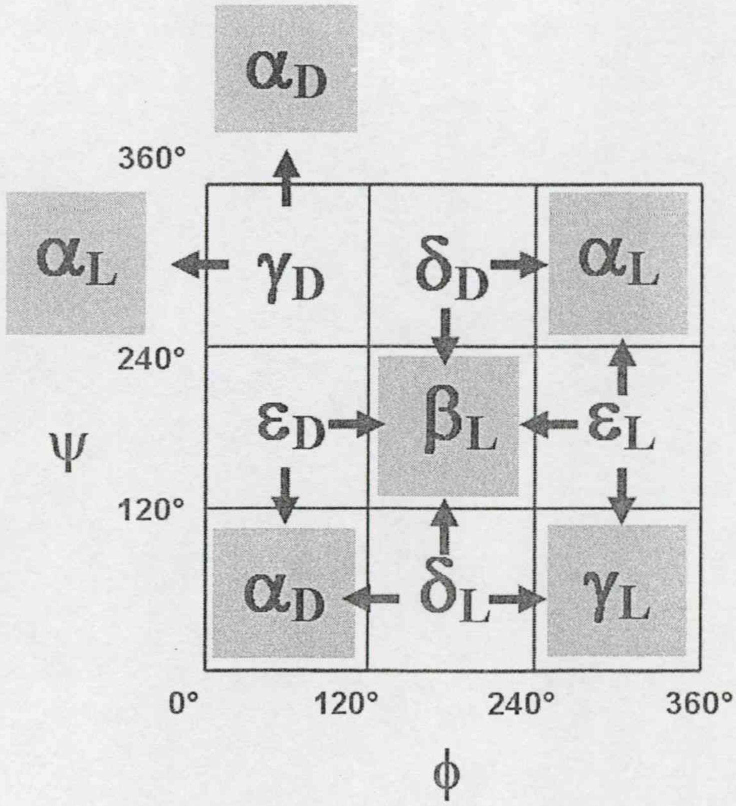

Figure 32 A schematic representation of the backbone conformational change of aspartic acid residue prior to sidechain deprotonation to the corresponding aspartate residue. Shaded areas represent stable aspartate conformations.

6. CONCLUSIONS

6.1 Aspartic Acid

6.1.1 Endo Form of Aspartic Acid

The conformational preferences for the *endo* form of **N**-acetyl-*L*-aspartic acid-**N'**-methylamide were determined by quantum chemical calculations at the B3LYP/6-31G(d) *ab initio* level. A total of 37 optimized stable conformers (out of the possible 81) were found for the aspartic acid residue at this level of theory. All relative energies, including the stabilization exerted by the sidechain on the backbone, have been calculated for the 37 stable conformers.

For this particular aspartic acid residue, various BB/BB (N-H····· O=C) and BB/SC (N-H····· O=C; N-H····· OH) hydrogen bonds were analyzed (**Figure 33**). There exists a SC/SC interaction in all 37 stable conformers, indicating that this interaction is important for the general stabilization of the *endo* form of the aspartic acid residue. In addition, two BB/BB interactions and four SC/BB interactions were observed amongst the stable conformers. The internal hydrogen bonding may deem significant if the aspartyl residue were to participate in intra- or inter- molecular interactions in polypeptides, such as in the RGD tripeptide. This is because these internal stabilizing forces may be disrupted to allow for the folding or unfolding of the overall polypeptide into a particular geometry.

In this work, the stable $g^- s^-$ conformer found at the α_L backbone may represent a novel geometry in which the aspartyl residue may arrange itself during such peptide folding.

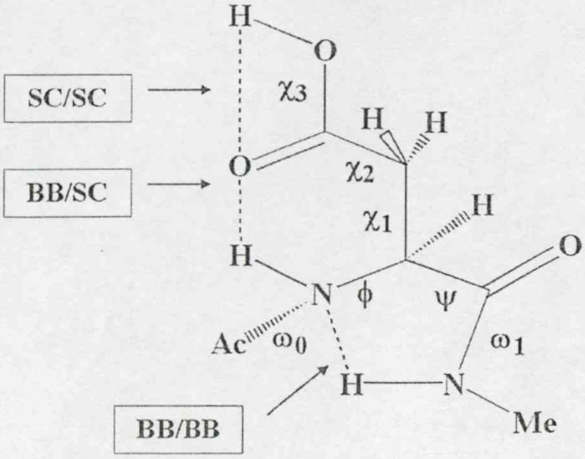

Figure 33 A schematic representation of the various hydrogen bond interactions that may exist in the *endo* form of the aspartic acid residue.

6.1.2 Exo Form of Aspartic Acid

Using quantum chemical calculations at the B3LYP/6-31G(d) *ab initio* level, the conformational preferences for the *exo* form of **N**-acetyl-*L*-aspartic acid-**N'**-methylamide were determined. A total of 27 stable conformers (out of the possible 81) were found for the aspartic acid residue at this level of theory. All relative energies, including the stabilization exerted by the sidechain on the backbone, were calculated for the 27 stable conformers.

Various BB/BB (N-H····· O=C) and BB/SC (N-H····· O=C; N-H····· OH) hydrogen bonds were analyzed (**Figure 34**). There was no SC/SC interaction in the carboxyl group of the aspartic acid residue, indicating that the sidechain may be involved in external hydrogen bonding to stabilize the amino acid. A total of two BB/BB interactions and six SC/BB interactions were identified amongst the stable conformers. However, only five of the possible six SC/BB interactions were observed. In addition, 25 of the 27 conformers exhibited at least one or more hydrogen bond types. External hydrogen interactions are significant when the aspartyl residue participates in intra- or inter- molecular interactions in polypeptides, such as in the RGD tripeptide. In the case of RGD, the presence or absence of these external stabilizing forces will directly affect the folding or unfolding of the tripeptide moiety.

In this work, the stable $g^- g^+$ conformer found at the ε_L backbone may represent a novel geometry in which the aspartyl residue may arrange itself during such peptide folding.

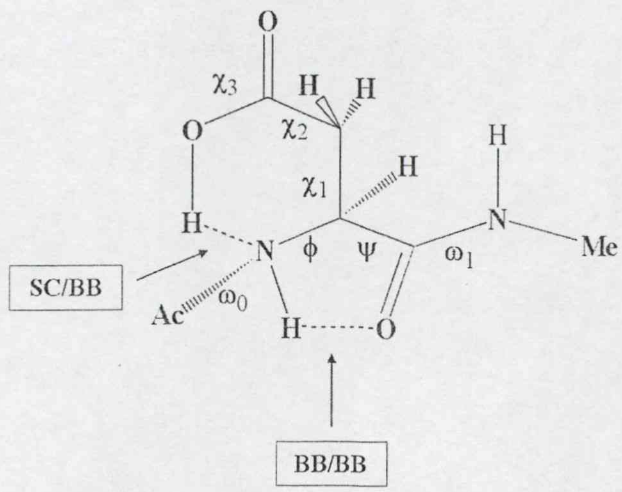

Figure 34 A schematic diagram showing the various hydrogen bond interaction that may exist for the *exo* form of the aspartic acid residue.

6.2 Aspartate Ion

Only 7 of the initially expected 81 conformers (located at the γ_L, β_L, α_L , and α_D backbone conformations) were found for **N**-acetyl-*L*-aspartate-**N'**-methylamide at the B3LYP/6-31G(d) level of theory. No conformers could be found in the δ_L, ε_L, γ_D, δ_D, and ε_D backbones. By comparing the relative energies of the *endo* and *exo* forms of **N**-acetyl-*L*-aspartic acid-**N'**-methylamide against those of **N**-acetyl-*L*-aspartate-**N'**-methylamide, the "adiabatic" deprotonation energies for the aspartic acid residue were found. The deprotonation patterns of the *endo* and *exo* forms of **N**-acetyl-*L*-aspartic acid-**N'**-methylamide with respect to **N**-acetyl-*L*-aspartate-**N'**-methylamide were established. It was found that the aspartic acid residue would rather change conformation to the favourable backbone structures (γ_L, β_L, α_L, α_D) before it would undergo deprotonation (**Figure 35**).

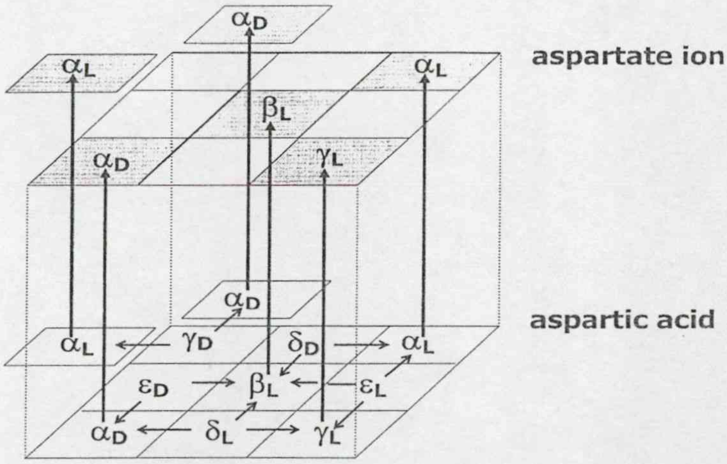

Figure 35
Deprotonation scheme of aspartic acid residue to aspartate ion.

The sidechain PEHS for the "vertical" deprotonation energies of the *endo* and *exo* forms of **N**-acetyl-*L*-aspartate-**N'**-methylamide showed similarities as well as difference in the deprotonation patterns between the two forms. Two types of hydrogen bond interactions were found for **N**-acetyl-*L*-aspartate-**N'**-methylamide: backbone-sidechain (N-H····· $^{-}$O-C) and backbone-backbone (N-H····· O=C). In sum, there were a total of 2 backbone-backbone and 4 backbone-sidechain interactions for the aspartate residue. These hydrogen bond interactions may help explain the geometric preference of RGD during peptide folding as well as the importance of the aspartyl residue during such molecular processes as ligand binding and ligand recognition by cell receptors.

7. REFERENCES

1. M. L. Lopez-Rodriguez, B. Vicente, X. Deupi, S. Barrondo, M. Olivella, M. J. Morcillo, B. Behamu, J. A. Ballesteros, J. Salles, L. Pardo; Mol. Pharmacol. 62 (2002) 15.

2. M. T. Makhija, V. M. Kulkarni; J. Comput. Aid Mol. Des. 15 (2001) 961..

3. I. Halperin, B. Ma, H. Wolfson, R. Nussinov; Proteins 47 (2002) 409.

4. M. Glick, D. D. Robinson, G. H. Grant, W. G. Richards; J. Am. Chem. Soc. 124 (2002) 2337.

5. J. Zhu, H. Fan, H. Liu, Y. Shi; J. Comput. Aid Mol. Des. 15 (2001) 979.

6. R. Bitetti-Putzer, D. Joseph-McCarthy, J. M. Hogle, M. Karplus; J. Comput. Aid Mol. Des. 15 (2001) 935.

7. A. W. Ravna, O. Edvardsen; J. Mol. Graph. Model. 20 (2001) 133.

8. O. A. Santos-Filho, R. K. Mishra, A. J. Hopfinger; J. Comput. Aid Mol. Des. 15 (2001) 787.

9. A. Percel, J. G. Ángyán, M. Kajtár, W. Viviani, J. L. Rivail, J. F. Marcoccia, I. G. Csizmadia; J. Am. Chem. Soc. 113 (1991) 6256.

10. M. A. McAllister, A. Perczel, P. Császár, W. Viviani, J. L. Rivail, I. G. Csizmadia; THEOCHEM 288 (1993) 161.

11. M. A. McAllister, A. Perczel, P. Császár, I. G. Csizmadia; THEOCHEM 288 (1993) 181.

12. A. Perczel, M. A. McAllister, P. Császár, I. G. Csizmadia; Can. J. Chem. 72 (1994) 2050.

13. M. Cheung, M. E. McGovern, T. Jin, D. C. Zhao, M. A. McAllister, A. Perczel, P. Császár, I. G. Csizmadia; THEOCHEM 309 (1994) 151.

14. A. M. Rodriguez, H. A. Baldoni, F. Suvire, R. Nieto-Vasquez, G. Zamarbide, R. D. Enriz, Ö. Farkas, A. Perczel, I. G. Csizmadia; THEOCHEM 455 (1998) 275.

15. M. Berg, S. J. Salpietro, A. Perczel, Ö. Farkas, I. G. Csizmadia; THEOCHEM 504 (2000) 127.

16. M. A. Zamora, H. A. Baldoni, J. A. Bombasaro, M. L. Mak, A. Perczel, Ö. Farkas, R. D. Enriz; THEOCHEM 540 (2001) 271.

17. M.A. Zamora, H.A. Baldoni, A.M. Rodriguez, R.D. Enriz, C.P. Sosa, A. Perczel, A. Kucsman, O. Farkas, E. Deretey, J.C. Vank, I.G. Csizmadia; Can. J. Chem. 80 (2002) 832.

18. A. Perczel, Ö. Farkas, I. G. Csizmadia; J. Am. Chem. Soc. 117 (1995) 1653.

19. H. A. Baldoni, G. N. Zamarbide, R. D. Enriz, E. A. Jauregui, Ö. Farkas, A. Perczel, S. J. Salpietro, I. G. Csizmadia; THEOCHEM 500 (2000) 97.

20. Ö. Farkas, M. A. McAllister, J. H. Ma, A. Perczel, M. Hollósi, I. G. Csizmadia; THEOCHEM 369 (1996) 105.

21. A. Perczel, Ö. Farkas, I. G. Csizmadia; Can. J. Chem. 75 (1997) 1120.

22. I. Jakli, A. Perczel, Ö. Farkas, M. Hollosi, I. G. Csizmadia; THEOCHEM 455 (1998) 303.

23. H. A. Baldoni, A. M. Rodriguez, G. Zamarbide, R. D. Enriz, Ö. Farkas, P. Csaszar, L. L. Torday, C. P. Sosa, I. Jakli, A. Perczel, M. Hollosi, I. G. Csizmadia; THEOCHEM 465 (1999) 79.

24. J. C. Vank, C. P. Sosa, A. Perczel, I. G. Csizmadia; Can. J. Chem. 78 (2000) 395.

25. A. Perczel, Ö. Farkas, I. G. Csizmadia; J. Comp. Chem. 17 (1996) 821.

26. A. Perczel, Ö. Farkas, I. G. Csizmadia; J. Am. Chem. Soc. 118 (1996) 7809.

27. I. Jakli, A. Perczel, Ö. Farkas, C. P. Sosa, I. G. Csizmadia; J. Comp. Chem. 21 (2000) 626.

28. W. Viviani, J-L. Rivail, A. Perczel, I. G. Csizmadia; J. Am. Chem. Soc. 115 (1993) 8321.

29. G. A. Chass, M. A. Sahai, J. M. S. Law, S. Lovas, Ö. Farkas, A. Perczel J.-L. Rivail I.G. Csizmadia; Int. J. Quantum Chem. P. Ö. Löwdin Memorial Issue 90 (2002) 933.

30. S. Hatse, K. Princen, L. O. Gerlach, G. Bridger, G. Henson, E. De Clercq, T. W. Schwartz, D. Schols; Mol. Pharmacol. 60 (2001) 164.

31. C. Demougeot, P. Garnier, C. Mossiat, N. Bertrand, M. Giroud, A. Beley, C. Marie; J. Neurochem. 77 (2001) 408.

32. K. Chlebovská, O. Chlebovský; Mech. Ageing Devel. 108 (1999) 127.

33. P. Fedoročko, N. O. Macková, Z. Šándorčínová-Hoferová, Z. Sedláková-Hoferová, P. Solár, O. Chlebovský; Mech. Ageing Devel. 119 (2000) 159.

34. J. A. Contreras, M. Karlsson, T. Østerlund, H. Laurell, A. Svensson, C. Holm; J. Biol. Chem. 271 (1996) 31426.

35. G. F. Short 3rd, A. L. Laikhter, M. Lodder, Y. Shayo, T. Arslan, S. M. Hecht; Biochemistry 39 (2000) 8768.

36. R. Hu, J. Bekisz, H. Schmeisser, P. McPhie, K. Zoon; J. Immunol. 167 (2001) 1482.

37. R. Hoffmann, D. J. Craik, K. Bokonyi, I. Varga, L. Otvos Jr.; J Pept Sci. 5 (1999) 442.

38. D. Saadat, D. H. Harrison; Biochemistry 37 (1998) 10074.

39. J. Rotonda, M. Garcia-Calvo, H. G. Bull, W. M. Geissler, B. McKeever, N. A. Thornberry, J. W. Becker; Chem. Biol. 8 (2001) 357.

40. M. J. Collins, E. R. Waite, A.C. van Duin; Philos. Trans. R. Soc. Lond. B. Biol. Sci. 354 (1999) 51.

41. M. A. Berg, G. A. Chass, E. Deretey, A. K. Füzéry, B. M. Fung, D. Y. K. Fung, H. Henry-Riyad, A. C. Lin, M. L. Mak, A. Mantas, M. Patel, I. V. Repyakh, M. Staikova, S. J. Salpietro, T.-H. Tang, J. C. Vank, A. Perczel, Ö, Farkas, L. L. Torday, Z. Székely, I. G. Csizmadia; THEOCHEM 500 (2000) 5.

42. E. Ruoslahti, M.D. Pierschbacher; Science 238 (1987) 491.

43. M. K. Magnusson, S. S. Hong, P. Boulanger, L. Lindholm; J. Virol. 75 (2001) 7280.

44. N. Okada, Y. Tsukada, S. Nakagawa, H. Mizuguchi, K. Mori, T. Saito, T. Fujita, A.Yamamoto, T. Hayakawa, T. Mayumi; Biochem. Biophys. Res. Commun. 282 (2001) 173.

45. C. Hay, H. De Leon, J. D. Jafari, J. L. Jakubczak, C. A. Mech, P. L. Hallenbeck, S. K. Powell, G. Liau, S. C. Stevenson; J. Vasc. Res. 38 (2001) 315.

46. C. D. Anuradha, S. Kanno, S. Hirano; Cell Biol. Toxicol. 16 (2000) 275.

47. H. Ghandehari, R. Sharan, W. Rubas, W. M. Killing; J. Pharm. Pharm. Sci. 4 (2001) 32.

48. D. Boehning, D. O. Mak, J. K. Foskett, S. K. Joseph; J. Biol. Chem., 276 (2001) 13509.

49. D. W. Shin, J. Ma, D. H. Kim; FEBS Lett. 486 (2000) 178.

50. B. Nilius, R. Vennekens, J. Prenen, J. G. Hoenderop, G. Droogmans, R. J. Bindels; J. Biol. Chem. 276 (2001) 1020.

51. S. J. Salpietro, A. Perczel, Ö. Farkas, R. D. Enriz, I. G. Csizmadia; THEOCHEM 497 (2000) 39.

52. J. C. P. Koo, G. A. Chass, A. Perczel, Ö. Farkas, L. L. Torday, A. Varro, J. G. Papp, I. G. Csizmadia; Eur. Phys. J. D 20 (2002) 499.

53. J. C. P. Koo, G. A. Chass, A. Perczel, Ö. Farkas, L. L. Torday, A. Varro, J. G. Papp, I. G. Csizmadia; J. Phys. Chem. A 106 (2002) 6999.

54. J. C. P. Koo, J. S.W. Lam, G. A. Chass, S. J. Salpietro, R. D. Enriz, L. L. Torday, A. Varro, J. Gy. Papp; THEOCHEM (2002) in press.

55. J. C. P. Koo, J. S.W. Lam, G. A. Chass, A. Perczel, Ö. Farkas, L. L. Torday, A. Varro, J. Gy. Papp; THEOCHEM (2002) in press.

56. GAUSSIAN 94, Revision D.2, M.J. Frisch, G.W. Trucks, H.B. Schlegel, P.M. W. Gill, B.G. Johnson, M.A. Robb, J.R. Cheeseman, T. Keith, G.A. Petersson, J.A. Montgomery, K. Raghavachari, M.A. Al-Laham, V.G. Zakrzewski, J.V. Ortiz, J.B. Foresman, J. Cioslowski, B.B. Stefanov, A. Nanayakkara, M. Challacombe, C.Y. Peng, P.Y. Ayala, W. Chen, M.W. Wong, J.L. Andres, E.S. Replogle, R. Gomperts, R.L. Martin, D.J. Fox, J.S. Binkley, D.J. Defrees, J. Baker, J.P. Stewart, M. Head-Gordon, C. Gonzalez, J.A. Pople, Gaussian, Inc., Pittsburgh Pa, 1995.

57. GAUSSIAN 98 (Revision A.*x*), M. J. Frisch, G. W. Trucks, H. B. Schlegel, G. E. Scuseria, M. A. Robb, J. R. Cheeseman, V. G. Zakrzewski, J. A. Montgomery, Jr., R. E. Stratmann, J. C. Burant, S. Dapprich, J. M. Millam, A. D. Daniels, K. N. Kudin, M. C. Strain, O. Farkas, J. Tomasi, V. Barone, M. Cossi, R. Cammi, B. Mennucci, C. Pomelli, C. Adamo, S. Clifford, J. Ochterski, G. A. Petersson, P. Y. Ayala, Q. Cui, K. Morokuma, D. K. Malick, A. D. Rabuck, K. Raghavachari, J. B. Foresman, J. Cioslowski, J. V. Ortiz, A. G. Baboul, B. B. Stefanov, G. Liu, A. Liashenko, P. Piskorz, I. Komaromi, R. Gomperts, R. L. Martin, D. J. Fox, T. Keith, M. A. Al-Laham, C. Y. Peng, A. Nanayakkara, C. Gonzalez, M. Challacombe, P. M. W. Gill, B. G. Johnson, W. Chen, M. W. Wong, J. L. Andres, M. Head-Gordon, E. S. Replogle and J. A. Pople, Gaussian, Inc., Pittsburgh PA, 1998.

58. M. Tarditi, M. W. Klipfel, A. M. Rodriguez, F. D. Suvire, G. A. Chasse, Ö. Farkas, A. Perczel, R. D. Enriz; THEOCHEM 545 (2001) 29.

59. M. F. Masman, M. G. Amaya, A. M. Rodriguez, F. D. Suvire, G. A. Chasse, Ö. Farkas, A. Perczel, R. D. Enriz; THEOCHEM 543 (2001) 203.

60. M. N. Barroso, E. S. Cerutti, A. M. Rodriguez, E. A. Jauregui, Ö. Farkas, A. Perczel, R. D. Enriz; THEOCHEM 548 (2001) 21.

61. C. M. Deane, F. H. Allen, R. Taylor, T. L. Blundell; Protein Eng. 12 (1999) 1025.

8. APPENDIX

Published and Accepted Papers

1. Exploration of the 4D-conformational potential energy hypersurface of N-acetyl-L-aspartic acid-N'-methylamide with its internally hydrogen bonded sidechain orientation, J. Phys. Chem. A, 106 (**2002**), 6999-7009.

2. N-acetyl-L-aspartic acid-N'-methylamide with sidechain orientation capable of external hydrogen bonding. Backbone and sidechain folding, studied at the DFT level of quantum theory, Eur. Phys. J. D 20 (**2002**), 499-511.

3. How Reliable Could Economic Hartree-Fock Computations Be In Studying Large, Folded Peptides? A comparative HF and DFT study on N- and C-protected aspartic acid, THEOCHEM **2002** (in press)

4. Conformational dependence of the intrinsic acidity of the aspartic acid residue sidechain in N-acetyl-*L*-aspartic acid-N'-methylamide, THEOCHEM **2002** (in press)